RESEARCH ARTICLE

VOLCANICA

A robust quantification of H_2O in silicate glasses through micro-Raman spectroscopy: insights on the compositional effect

Filippo Ridolfi*[α] and Diego González-García[α,β]

[α] Institute for Earth System Sciences, Leibniz Universität Hannover, Hannover, Germany.
[β] Department of Mineralogy and Petrology, Universidad Complutense de Madrid, Madrid, Spain.

Submitted: 2024-09-16 | Accepted: 2025-05-08 | Published: 2025-07-25

Editor: L. Elkins | Typesetter: E. Hughes

Abstract

Micro-Raman spectroscopy is considered one of the most promising, rapid and economical methods to measure the water content in small volumes (a few μm^3) of natural glasses (e.g. volcanic glass matrix and melt inclusions in minerals), which is a fundamental parameter to obtain information and constraints on the feeding systems of volcanoes. In this article we report a new method for calibrating micro-Raman spectroscopy for water determination based on the analysis of a large number of silicate glasses (101) synthesized over a wide compositional (basalt, basaltic andesite, andesite, haplogranite, shoshonite, latite and phonolite) and physico-chemical range (T = 1000–1275 °C, P = 50–500 MPa, fO_2 = ±2.6 log units from the Ni-NiO buffer) with H_2O contents between 0.2 and 7.6 ±0.1 wt.%. A robust and reproducible method for baseline subtraction and measurement of the water and silicate areas and their ratio ($R_{w/s}$) is proposed. $R_{w/s}$ data show an average error of ±0.07 confirming the high potential of Raman spectroscopy of accurately determining the water content. Regression analysis allows the achievement of improved water equations as a function of $R_{w/s}$ and the anhydrous composition of the glasses, accounting for relatively low H_2O uncertainties (average error = 0.16–0.17 wt.%; standard error of the estimate, σ_{est}, = 0.21–0.22 wt.%) compared to previous calibrations based on smaller compositional ranges and sample numbers. These equations are reproducible and easily applicable to both experimental and natural glasses. Our analyses also indicate that the H and H/Σcations (hydrogen and sum of other cations, calculated on the 8-oxygen basis) vs. $R_{w/s}$ relationships are affected by the amount of trivalent (Al^{3+} and Fe^{3+}) and pentavalent (P^{5+}) cations. This hypothesis requires additional investigations as, at the state of the art, the estimate of Fe^{3+}/Fe^{2+} in experimental glasses is not sufficiently accurate.

Non-technical summary

In-situ determination of water content (in a few μm^2) in volcanic glasses is one of the fundamental parameters to obtain constraints on the feeding systems of volcanoes. In this article we report a new method for calibrating micro-Raman spectroscopy for water determination based on the analysis of a large number of hydrous silicate glasses synthesized in wide compositional and phyisico-chemical ranges. Our analysis indicate that the water determination by Raman is affected by the amount of trivalent (Al^{3+} and Fe^{3+}) and pentavalent (P^{5+}) cations in the glass. Regression analysis allowed us to achieve equations dependent on Raman spectroscopy and the glass composition accounting for relatively low H_2O uncertainties (±0.21–0.22 wt.%) that are easily applicable to natural glasses. This information is crucially needed to obtain the storage conditions and processes of subvolcanic magma systems, leading the scientific community towards a better understanding of the mechanisms that triggers eruptions.

Keywords: Raman spectra processing; EPMA analysis; Compositional effects; Regression analyses; In-situ water quantification; Melt inclusions.

1 Introduction

A micro-analytical tool to accurately quantify water content with high spatial resolution (a few μm^2) of glass is extremely important in petrology and volcanology, in particular for characterizing the processes and conditions of magma feeding systems. For instance, in fluid-undersaturated rocks (e.g. cordierite-bearing anatectic rhyolites and granites) and H_2O-CO_2 saturated calc-alkaline products (e.g. lavas and pyroclastic products), the H_2O concentration in glass inclusions is an essential parameter to estimate the magmatic physico-chemical conditions (pressure, P; temperature, T; and oxygen fugacity, fO_2) of melt entrapment and constrain the genesis of plutonic rocks, magma storage and the processes governing the eruptions of active and quiescent volcanoes [Webster et al. 2003; Blundy et al. 2006; Blundy and Cashman 2008; Metrich and Wallace 2008; Moore 2008; Gaetani et al. 2012; Ridolfi et al. 2014; 2016; Konzett et al. 2018; Giordano et al. 2020; González-García et al. 2021]. In addition, H_2O in the matrix glass plays a fundamental role in assessing volatile budgets, the kinetics of diffusion processes associated with magma mixing/mingling processes, crystal growth and dissolution, and to model the rare earth and high field strength element patterns due to fractional crystallization [e.g. González-García et al. 2017; 2018; Mollo et al. 2018; González-García et al. 2024]. In addition, an accurate *in-situ* determination of H_2O in glasses is essential to fully characterize experimental petrology products and reduce the uncertainty of derived thermobarometric and diffusive models which, in turn, are crucially needed to obtain the storage conditions and processes of subvolcanic magma systems [e.g. Ridolfi et al. 2010; González-García et al. 2017; 2018; Ridolfi et al. 2023; Bamber et al. 2024].

* filippo.ridolfi@uniurb.it

Secondary ion mass spectrometry (SIMS) and Fourier transform infrared spectroscopy (FTIR) are traditionally used for this task but they can be expensive, time consuming, require extensive sample preparation and/or be destructive [e.g. Behrens et al. 1996; Humphreys et al. 2006]. In contrast, confocal micro-Raman spectroscopy has great potential as a user-friendly tool for an accurate *in-situ* determination of water in glasses as it requires little sample preparation and is an affordable, fast and non-destructive method with similar or higher spatial resolution. Because of this, the application of Raman in the fields of petrology and volcanology has seen a sustained increase over the last decades.

A generalized robust calibration using well-characterized standards is required for the accurate quantification of dissolved H_2O in silicate glasses, although each calibration appears unique depending on the Raman spectrometer used [e.g. Shea et al. 2014]. Both external and internal calibrations have been employed for this purpose. External calibration consists in directly correlating the integrated area of water spectra peaks (water intensity), peaking at 3550 cm^{-1}, with the measured amount of H_2O [Behrens et al. 2006]. In the internal method the intensities or areas of the water band are normalized to those of the silicate region (two main bands between 100 and 1400 cm^{-1}) and then correlated to the H_2O concentration [e.g. Le Losq et al. 2012]. The internal calibration is generally preferred as it increases reproducibility and reduces the effect of analytical conditions and instrumental set-up such as laser power or counting time, among others [e.g. Behrens et al. 2006; Mercier et al. 2009; Le Losq et al. 2012; Van Gerve and Namur 2023].

A key step in spectroscopic calibrations is to correctly remove the background signal of the collected Raman spectra. Several empirical methods have been proposed for this purpose [e.g. Zajacz et al. 2005; Behrens et al. 2006; Di Muro et al. 2009; Mercier et al. 2009; Zhang et al. 2010; Le Losq et al. 2012; Schiavi et al. 2018; Giordano et al. 2020; González-García et al. 2021; Tu et al. 2023]. All these methods present some degree of arbitrariness due to the fact that both silicate and water peak components change their shape and intensity with the glass composition itself (i.e. anhydrous element-oxides, water content and oxidation state of iron) [e.g. Behrens et al. 2006; Le Losq et al. 2012; Di Genova et al. 2015; 2017; Schiavi et al. 2018; González-García et al. 2020; Bonechi et al. 2022]. In addition, the fact that different procedures were adopted in recent publications indicates that the background signal removal is not a straightforward procedure and is subject to interpretation [Van Gerve and Namur 2023]. Conceivably, an alternative method for background removal in the water region would be to subtract a dry glass spectrum. This procedure is not really feasible because it would require a large amount of data elaboration and sample preparation. In addition, in the silicate region, the complex relationship between the shape of the spectra and their chemical composition (and structure) yields any modeling based on the spectra of glasses with a simple composition and/or on structural computing particularly difficult and impractical. In this paper, we propose a strict and reproducible internally consistent method for a correct removal of the background signal based on the maximization of the area of both water and silicate peak regions, by using the user-friendly program `SilicH2O` [Van Gerve and Namur 2023]. In addition, we analyze the main glass formula parameters affecting the relationship between H concentration and the Raman ratio between water and silicate areas. With this respect, we show that the amount of trivalent (Al^{3+} and Fe^{3+}) and pentavalent (P^{5+}) cations plays a main role in the calibration and should be considered in future investigations.

We finally propose two compositionally-dependent regression methods removing biases observed for different glass compositions and resulting in uncertainty of water determination in silicate glasses consistent with that of the error propagation theory, which can be easily reproduced by any user and/or laboratory.

2 Analytical methods and data processing

2.1 Samples and compositional determinations

This work is based on the collection of a large number of H_2O-bearing glasses (N = 101; Supplementary Material 1) synthesized overtime at the Leibniz University of Hannover (LUH) using Internally Heated Pressure Vessels [IHPV; e.g. Behrens et al. 2006]. So far, this database is the largest considered for H_2O Raman calibration and mostly consists of mafic to intermediate subalkaline glasses [i.e. basalt to andesite, N = 89: Almeev et al. 2007; Shishkina et al. 2010; Almeev et al. 2012; Almeev et al. 2013; Koch et al. 2025, and other unpublished data], three unpublished synthetic haplogranitic glasses and one latite, and other alkaline glasses (shoshonite and phonolite) published by González-García et al. [2017, 2024] (Figure 1 and Supplementary Material 1).

The glass synthesis conditions are detailed in the above literature. In summary, natural volcanic rocks or mixtures of element-oxides were powdered, melted at 1600 °C in an ambient-pressure box furnace, quenched in air and powdered again. After repeating this procedure 2–4 times, to ensure chemical homogeneity, the glass powders and the target amount of H_2O were loaded in noble metal (Au, AuPd or Pt) capsules and run in different IHPVs at super-liquidus conditions (1000–1275 °C, 50–500 MPa) and intrinsic fO_2 conditions [1.5–2.6 ΔNNO; where ΔNNO is $\log fO_2 - \log fO_2$ at Ni-NiO buffer, Hirschmann et al. 2008] for durations spanning from a few hours to a few days. Experiments were terminated by a rapid quench device [Berndt et al. 2002], achieving high cooling rates and preventing crystallization.

After quenching, glass chips were mounted in 1-inch round epoxy stabs or thin sections for compositional and H_2O determinations. Glass element-oxide compositions were determined by an Electron Probe Micro Analyzer (EPMA) and H_2O contents were quantified by FTIR in double-polished thin sections. Other glass chips were selected for H_2O determination via Karl Fischer Titration (KFT). FTIR and KFT water determinations were performed according to established methodologies in Hannover [e.g. Behrens et al. 1996; Leschik et al. 2004; Behrens et al. 2009]. The uncertainty in H_2O concentration of FTIR is higher with respect to that of KFT, in particular for iron-bearing glasses [e.g. Le Losq et al. 2012]. For this reason, the selected H_2O content for our calibration is the

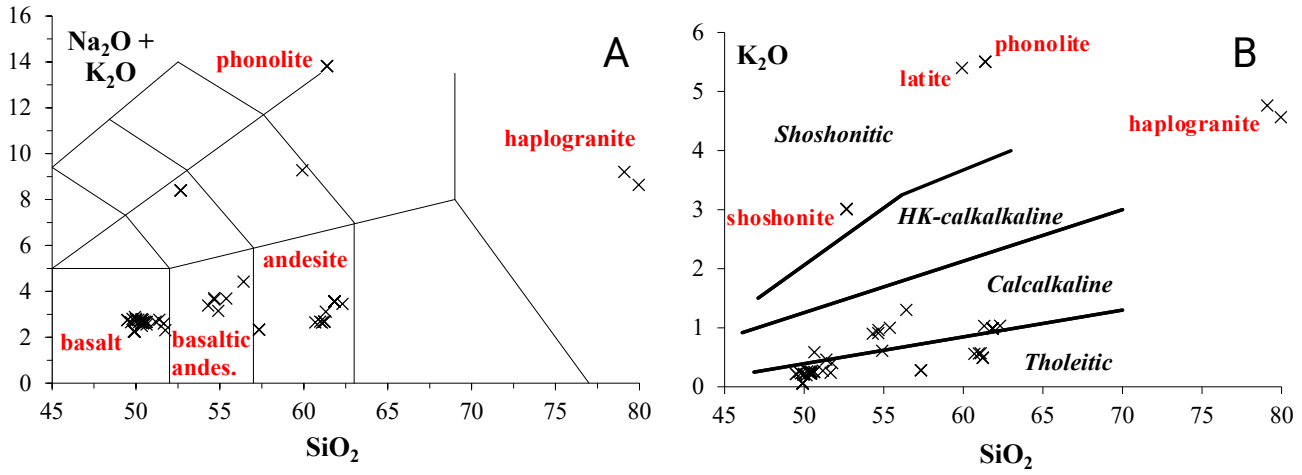

Figure 1: [A] TAS (Total Alkali vs. Silica) and [B] KS (K_2O vs. SiO_2) diagrams for the studied glasses (Supplementary Material 1). [B] shows the magmatic series in *italics* while the compositional classification names are reported in red in both diagrams.

one determined by KFT, obtained for 85% of the glasses. The remaining glasses in our database report FTIR water concentrations. The H_2O contents vary from 0.2 to 7.6 wt.% with estimated uncertainties between 0.02 and 0.28 wt.%, 0.10 wt.% on average. The glass database in Supplementary Material 1 includes four andesite glasses whose H_2O content is just nominal (i.e. the amount of H_2O loaded in the capsules run at fluid under-saturated conditions), due to technical issues preventing KFT water determination. These glasses are only used as testing data in this work (see Section 4.2).

EPMA was used to check for the absence of nano/microlites (through secondary and back-scattered electron imaging) and element-oxide quantification. For the unpublished glasses, we used the Cameca SX100 electron microprobe equipped with 5 spectrometers at LUH. Quantitative analyses were performed with a beam size of 20 µm (20 keV, 2 nA), maintaining a low current density (0.06 nA/µm^2) to minimize the loss of Na [e.g. Morgan VI and London 2005]. Typical (average) uncertainties vary with the amount of measured element-oxide according to the equation $\sigma\% = 5.762X–0.66$, where X is the average element-oxide wt.% and σ% is the standard deviation percentage of multiple measurements in different parts of the glass chips [i.e. σ% = σ wt.%/X Ridolfi et al. 2023].

To estimate the amounts of Fe_2O_3 and FeO in the glasses, we used the EPMA composition and synthesis P-T conditions to first estimate the water activity (i.e. a_{H2O}) through the Burnham model [Burnham 1994], hence the effective fO_2 condition by the equation $\log fO_2 = \log fO_2$[intrinsic] (i.e. at a hypothetical $a_{H2O} = 1$) $- 2\log a_{H2O}$ [e.g. Botcharnikov et al. 2005; 2008; Almeev et al. 2013]. Finally, the Fe_2O_3/FeO ratio was estimated using the model of Jayasuriya et al. [2004]. This complete characterization is available for 92 of the glasses, spanning a large compositional range (basalt, basaltic andesite, andesite, shoshonite, latite, phonolite, haplogranite; Supplementary Material 1 and Figure 1). For the remaining eight glasses the experimental physico-chemical conditions (P-T-fO_2) are not available or EPMA measurements were not performed, although their starting materials have basaltic composition (Supplementary Material 1).

2.2 Micro-Raman spectroscopy

Raman spectra of the synthesized experimental glasses were acquired using a Bruker Senterra II confocal integrated micro-Raman system installed at the Section of Mineralogy of the Institute of Earth System Sciences, LUH. The spectrometer is equipped with a Peltier-cooled CCD detector coupled to an Olympus optical microscope. The excitation source is a solid-state Nd-YAG laser with a wavelength of 532 nm (green light) and a power of 20 mW. Spectra were acquired in the 70–4400 cm^{-1} range, with a spectral resolution of 9–15 cm^{-1}, using a 100× objective and an aperture of 50 µm. The analytical spot size is in the order of 1 µm. In each spot, 5 acquisitions of 30 s each were integrated. Under these conditions, the resulting laser power at the sample surface is expected to be in the order of 5 mW, i.e. low enough to avoid any H and Na migration [González-García et al. 2021]. Before glass measurements, the system was calibrated with a Si standard plate for peak position (frequency shift in cm^{-1}). Spectra were acquired using the Bruker `OPUS` software.

Among the resulting spectra, only those showing "glass-only" features were selected. Spectra showing signs of nanolitization, in the form of peak centred at ca. 670 nm, were excluded from the final database, as these features obliterate key parts of the spectrum and strongly affect the final calibration [Di Genova et al. 2017; Cáceres et al. 2021; González-García et al. 2021]. The raw spectra of all glasses are reported in Supplementary Material 2.

2.3 Raman spectra processing

After acquisition, raw spectra intensity was corrected for analytical conditions by using the expression of Long [1977]. This equation accounts for differences in temperature and laser excitation wavelength, and it is expressed as follows:

$$I = I_{\text{obs}} \left(\nu_0^3 \cdot \nu \frac{\left(1 - exp\left(-\frac{hc\nu}{kT}\right)\right)}{(\nu_0 - \nu)^4} \right), \quad (1)$$

where I_{obs} is the measured intensity, ν_0 is the excitation laser wavenumber in cm^{-1}, ν is the measured wavenumber, h is the Planck constant in J s, c is the speed of light in cm s^{-1}, k is the Boltzmann constant, and T is the sample temperature expressed in K.

The application of the Long [1977] correction to the measured spectra is not universally applied, and it has been suggested that, in some applications, it has no effect on the final quality of data [e.g. González-García et al. 2020; Van Gerve and Namur 2023]. However, our tests show that its application results in easier and more consistent baseline fitting of our spectra [as also noted by González-García et al. 2021].

The Long-corrected spectra were processed through the user-friendly `SilicH2O` software, that uniforms and streamlines the processing of Raman spectra by an interactive graphical interface [Van Gerve and Namur 2023]. It allows the user/operator to remove unwanted peaks by interpolation and unmixing, and set up water calibrations with reference glasses by loading and processing a group of spectra and exporting the results to a single datasheet. In addition, `SilicH2O` allows a real-time calculation of the amount of water (high frequency) and silicate (low frequency) areas, and their ratio (i.e. $R_{w/s}$), by an instant removal of the background signal. This procedure largely facilitates the task of choosing the best bands-setting for the calibration of the instrument through the H_2O concentration of a large number of standardized glasses (i.e. Supplementary Material 1).

3 Testing published methods of baseline subtraction

As a first approach, we considered several literature procedures of baseline subtraction obtained in a wide compositional range and using the same algorithm of `SilicH2O` [i.e. cubic smoothing splines; Van Gerve and Namur 2023]. Other algorithms giving different local curvatures (i.e. linear extrapolation [Zajacz et al. 2005] and interpolations with polynomials [Thomas et al. 2008], cubic splines [Behrens et al. 2006; Di Genova et al. 2017]) were not tested in this work as the overall baseline shape is mostly controlled by the selected anchor points [Di Muro et al. 2009; Van Gerve and Namur 2023]. Indeed, Giordano et al. [2020] pointed out that, in the silicate region, the inter-laboratory spectra changes are dominated by a variation of the measured intensity of the different Raman spectrometers due to the differences in spectral response of the instruments. The frequency shift, at which the anchor points are applied, is invariant between the different spectrometers as it is anchored to the peak of Si (see Section 2.3). Another criterion of testing selection is the strictness of the proposed method (i.e. the lack of arbitrary anchor points). For instance, some procedures, such as that of Schiavi et al. [2018], were discarded because the position of anchors points depends on the glass compositions (basanite, basalt, andesite, rhyolite) that were not quantitatively constrained.

One of the more generalized, promising and followed approach for Raman baseline subtraction and water calibration was proposed by Le Losq et al. [2012]. These authors analysed 12 glasses spanning a large compositional range (basalt to rhyolite with H_2O content of 0.1–11.7 wt.%) and proposed a "compositionally-independent" method to locate the Background Interpolation Regions (*BIRs*; i.e. regions of spectra exclusion delimited by lower and higher frequency anchor positions) and thus constrain the spline-cubic baselines from which a corrected spectrum is obtained by subtraction. From the resulting spectra, the water (high-frequency) and silicate (low-frequency) areas are finally measured. This method consists of constraining the baseline in the high-frequency region (i.e. the H_2O region at 2700–4000cm^{-1}) by placing two *BIRs* from 2700–2800 to 3100 cm^{-1} (a), and from 3750 to 4000 cm^{-1} (b). The beginning of the *BIR* (a) does not affect the shape of the baseline and water area, and it thus was placed at 2700 cm^{-1} for all our glass spectra. In the low-frequency region (i.e. the silicate framework bands at 0–1500 cm^{-1}), the first *BIR* is fixed at 20–150 cm^{-1} and one or two intermediate small *BIRs* are located at 600–900 cm^{-1} [Le Losq et al. 2012]. Their position and extension basically correspond to valley (depression) regions and depend on the glass chemistry. Le Losq et al. [2012] gave approximate indication of where to place these *BIRs* based on the SiO_2 content in the glasses. It is worth noting that this region is very complex and is potentially affected by other compositional factors such as the oxidation state of iron, and the concentration of alkalis and aluminium. To avoid any arbitrariness, we simply located one or two narrow intermediate *BIRs* to maximize the area of the silicate region. The last *BIR* in the low-frequency region also shows some degree of arbitrariness as it is placed from 1200–1300 to 1500 cm^{-1} [Le Losq et al. 2012]. According to these authors the beginning of this *BIR* depends on the degree of glass polymerization although quantitative constraints are not reported. Also in this case, we applied the principle of area maximization to locate the first anchor of this *BIR*. For the glasses in our database the start of this *BIR* falls within the 1250–1270 cm^{-1} range (e.g. Figure 2).

Figure 2 reports representative baseline-subtraction charts obtained by applying this method to our samples using the `SilicH2O` software. For the haplogranite, this method appears to work quite well in the low-frequency silicate region. In contrast, the baseline underneath the H_2O peak is bending up and does not apparently follow the pattern of the baseline before and after the peak that appears to continue to lower (~≤2700 cm^{-1}) and higher (~≥3800 cm^{-1}) frequencies, respectively (Figure 2A). Similar patterns can be observed for the andesite, basalt and latite (Figure 2B, 2C, and 2E, respectively). This indicates that the *BIRs* do not consider the low-wavenumber tail of the H_2O peak, most probably resulting in an underestimation of the water peak area. However, this behaviour is not observed for the phonolite and shoshonite (Figure 2C and 2E). Similar to the haplogranite, the baseline at the low-frequency region of the phonolite seems to correctly constrain the area of the silicate peaks (Figure 2D) whereas it bends above the spectra pattern for the remaining glasses and hence underestimates the silicate area (Figure 2B, 2C, 2E, and 2F).

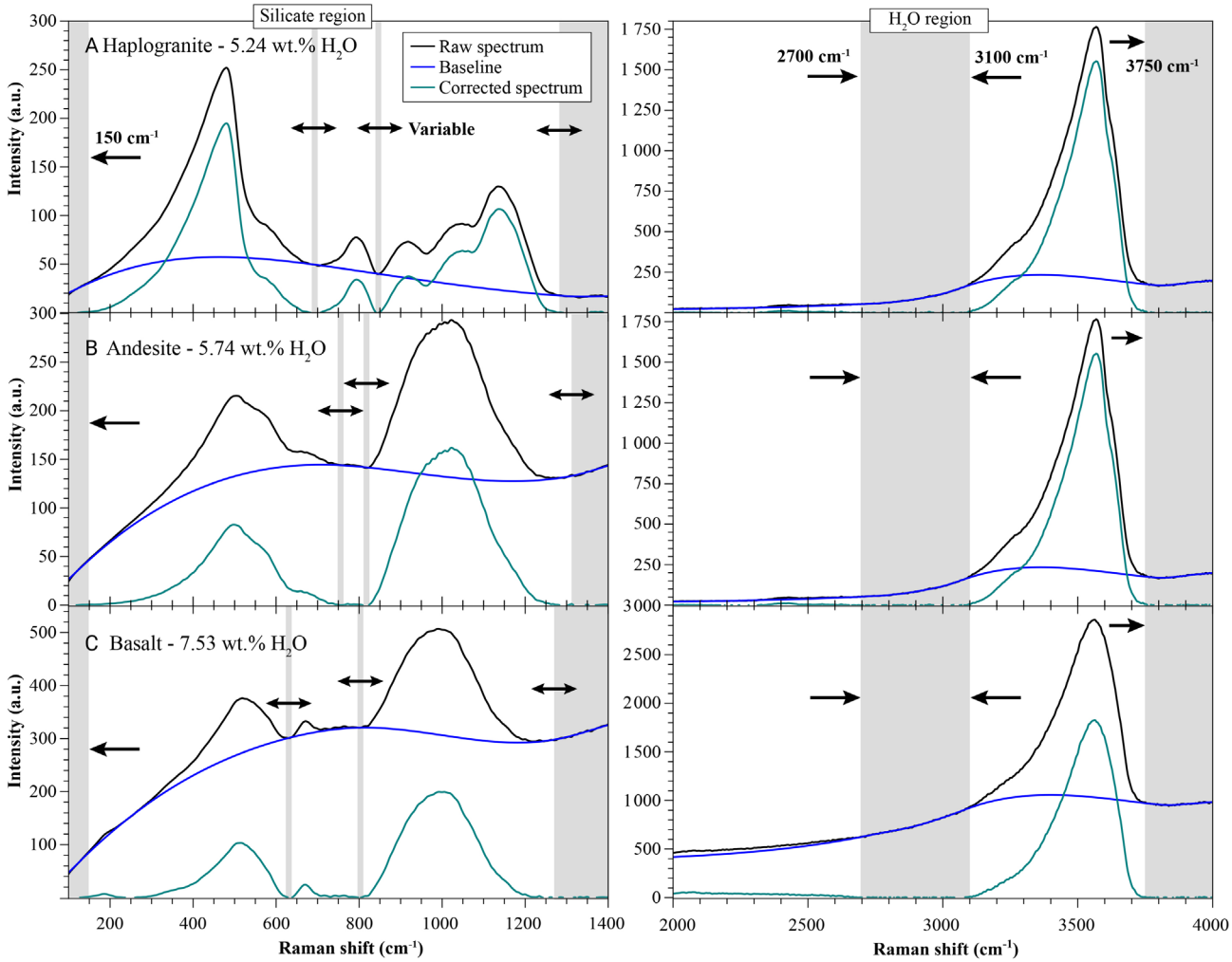

Figure 2: Application of the baseline subtraction method of Le Losq et al. [2012] to representative H_2O-bearing glass spectra using the SilicH2O program [Van Gerve and Namur 2023]. All plots show the variation of the intensity (arbitrary units, a.u.) with the Raman frequency shift (cm^{-1}). The original and subtracted (after baseline subtraction) Long-corrected patterns of the glass spectra are reported in black and green, respectively. *BIRs* are shaded grey bands with different extensions. Fixed and variable *BIR* limit positions are marked by black single and double arrows, respectively. (Continued on next page.)

Following Le Losq et al. [2012], the final calibration is obtained by fitting H_2O wt.%/(100–H_2O wt.%) with $R_{w/s}$ (Figure 3), where the use of the mass ratio should avoid correlation effects due to the analytical closure and the relative Raman contribution of glass water and silicate components [Aitchison 1986; Le Losq et al. 2012]. Applying this procedure to our database, we find that the correlation between $R_{w/s}$ and H_2O concentration results in a determination coefficient (R^2) of 0.88 (Figure 3A). Associated H_2O uncertainties are up to 3 wt.% and the standard error of the estimate (σ_{est}) is 0.7 wt.% (average error, i.e. AE = 0.5 wt.%). Forcing the intercept to the origin [Le Losq et al. 2012] has the only effect of increasing the uncertainty (R^2 =0.87). All of this indicates low accuracy of the method, especially for glasses with H_2O contents higher than ca. 3 wt.%.

Di Genova et al. [2017] also used an algorithm accounting for cubic smoothing splines and proposed a slightly different baseline subtraction method based on the analysis of a wide compositional range of nanolite-free, iron-bearing glasses (20 among basalts, trachy-basalts, latites, dacites, trachytes, rhyolites and phonolites; H_2O = 0.6-4.5 wt.%). These authors proposed a four fixed *BIRs* setup (i.e. 50-200, 1240-1500, 2750-3100, 3750-3900 cm^{-1}) and no intermediate narrow *BIRs* at the silicate region (600–900 cm^{-1}). The application of no intermediate *BIRs* is problematic for our haplogranite glass spectra as the baseline bends above the spectra resulting in large $R_{w/s}$ overstimations. For these spectra, we adopted two narrow *BIRs* [Di Genova, personal recommendation] using the area maximization criterion reported above (e.g. Figure 2A).

Similarly to Le Losq et al. [2012], the application of this method shows a bending up of the baseline underneath the H_2O peak (i.e. not considering the low-wavenumber tail of H_2O) for the haplogranite, andesite, basalt and latite spectra (e.g. Figure 2A, 2B, 2C, and 2E), resulting again in an underestimation of the water peak area. The H_2O content (wt.%) is finally obtained multiplying $R_{w/s}$ for a correcting coefficient accounting for the total iron content of the glasses (i.e. m = 0.096 × FeO_{tot} + 0.663), which is apparently independent on the used spectrometer as inferred by comparable σ_{est} (i.e. 0.29

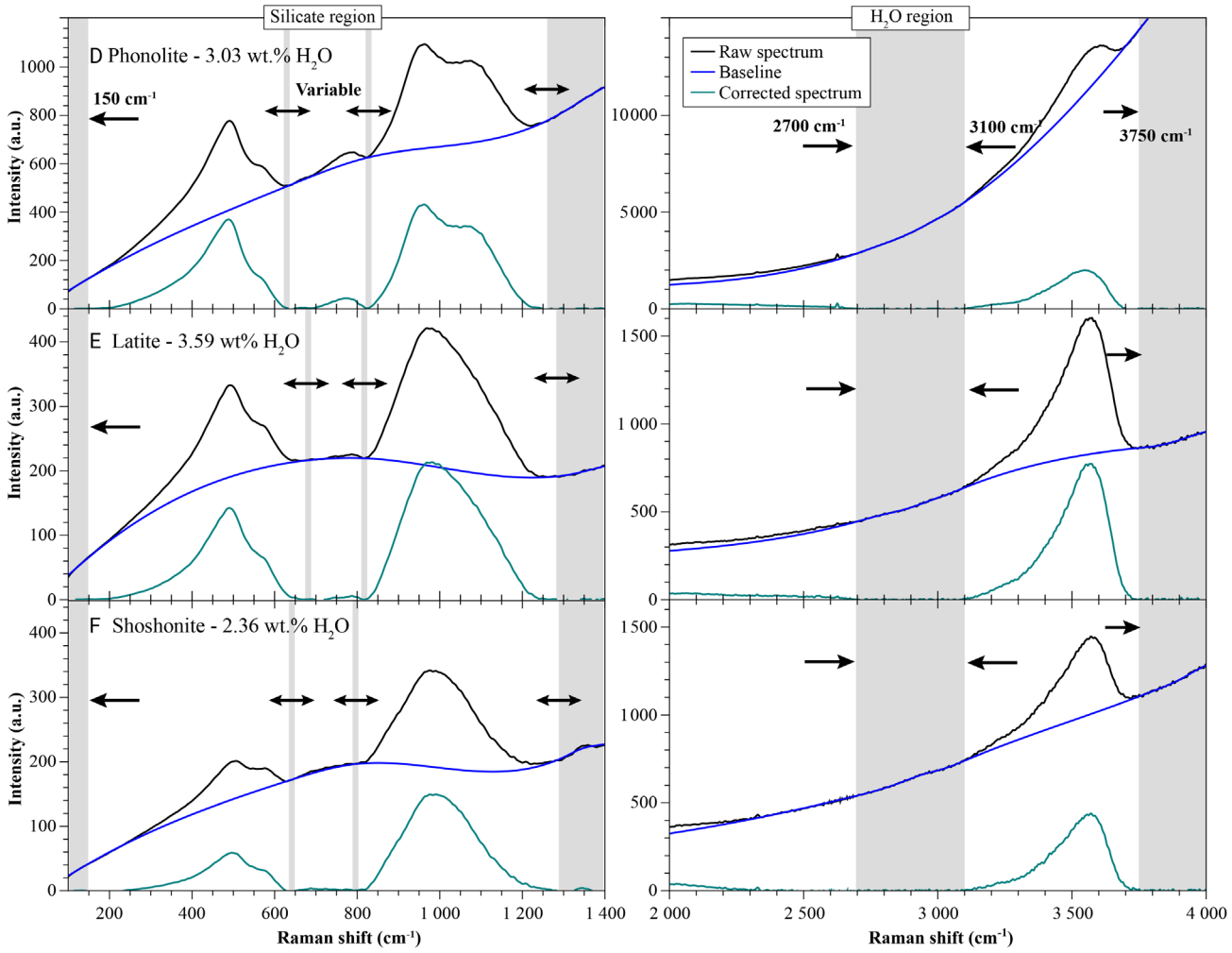

Figure 2: Continued.

and 0.47 wt.%) obtained with the use of two different spectrometers [Di Genova et al. 2017].

Figure 3B shows the correlation between the water content measured in this work and that estimated using the method of Di Genova et al. [2017]. The diagram shows a general water content overestimation (as shown by a slope lower than 1 of the linear correlation, i.e. 0.802) that increases with the amount of H_2O. Similarly to the method of Le Losq et al. [2012], H_2O uncertainties are up to 3.1 wt.% and σ_{est} is 0.8 wt.%, with no variations by excluding the haplogranite data. However, the correlation shows a determination coefficient (R^2) of 0.96, suggesting that the *m* coefficient changes with the used spectrometer and/or other compositional parameters [e.g. Bonechi et al. 2022]. To correct this, we retrieved a new iron-coefficient *m'* using our results (i.e. 0.056 × FeO_{tot} + 0.775) to be multiplied by the $R_{w/s}$ obtained by the application of the baseline subtraction method of Di Genova et al. [2017] (Figure 3C). Despite the low R^2 of this equation (i.e. 0.34; Figure 3C), the correlation between the measured water contents and those obtained with this modified version of Di Genova et al [2017] is largely improved and apparently erases the bias of the original method (Figure 3D). R^2 increases to 0.97 and the maximum uncertainty and σ_{est} decrease to 1.3 and 0.37 wt.%, respectively (AE = 0.25 wt.%) that are consistent with those reported by the authors (σ_{est} 0.29–0.47 wt.%).

It is worth noting that these uncertainties and those obtained with the application of Le Losq et al. [2012] are two to four times higher than those expected by the error propagation theory (Section 4.2).

4 Proposed baseline fitting method and error propagation

Based on the consideration reported above, we tested an improved and more constrained *BIR* setup to consistently extract the values of silicate and water areas, and thus the related $R_{w/s}$ ratio. To find an optimal treatment procedure, we first removed any peak due to contaminants such as air (2630 cm^{-1}; Figure 2B) and epoxy resin (2850–3120 cm^{-1}) using the interpolation method implemented in `SilicH2O`. The former occasionally occurs in any type of sample while epoxy peaks are sometimes found in round stub samples. Anomalous minor peaks of dubious origin (such as those at 1300–1400 and 2330 cm^{-1}) in the shoshonite spectrum were also removed (see Figure 2F).

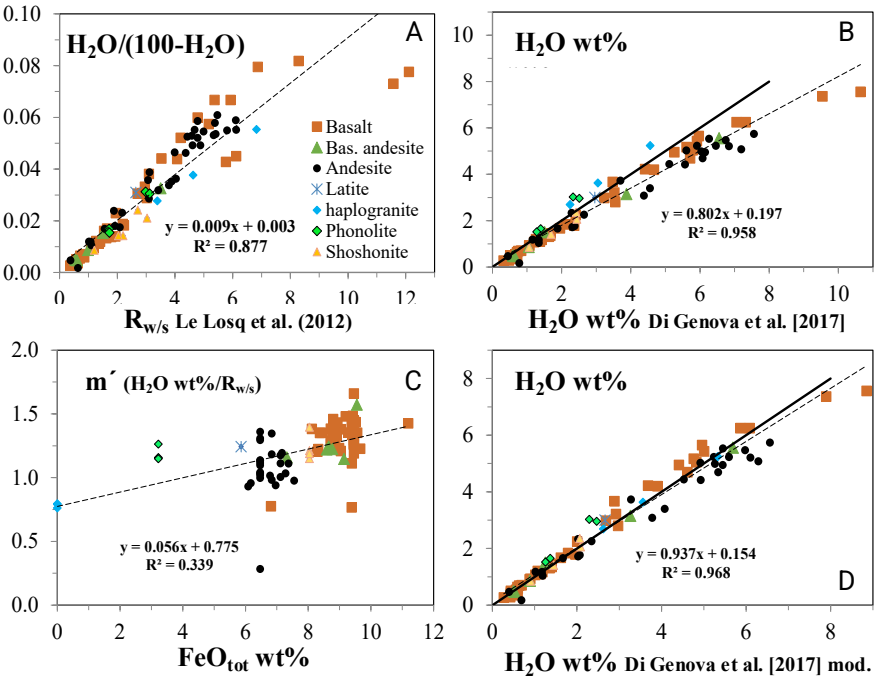

Figure 3: Test of the baseline subtraction methods of Le Losq et al. [2012] [A] and Di Genova et al. [2017] [B] using the sample database in this work. [C] Correlation of the *m'* coefficient (i.e. measured H_2O wt.%/$R_{w/s}$) with the anhydrous FeO_{tot} content for our glasses. [D] Correlation between the measured H_2O wt.% contents and those estimated with the modified version of Di Genova et al. [2017]. In all diagrams, the dashed lines show the correlation among the data while the bold solid lines in [B] and [D] show the 1:1 relation. See text for additional explanations.

The main criterion we adopted to obtain the following processing method is the maximization of the silicate and water area. This resulted in patterns of the baseline at the *BIRs* as "natural" as possible, i.e. a continuation of the previous and posterior spectra patterns (Figure 4). In other words, we aimed at finding the best *BIR* position and extension to keep the baseline slope constant before and after the *BIRs* limits (resulting in a lack of the apparition of swells and inflections under the silicate and water regions observed in other methodologies; e.g. Figure 2) obtaining the maximum water and silicate area values. After *BIR* selection, the applied baseline is in all cases that implemented in the `SilicH2O` software; i.e. a cubic spline calculated between the selected *BIRs* [Van Gerve and Namur 2023].

4.1 *BIR* constraints and tips

Figure 4 reports the application of this method to the representative glass spectra of Figure 2. Our procedure resulted in no apparent baseline bends below the H_2O peak, thus consistently avoiding the underestimation of the water area.

Our methodology consists of maintaining two fixed *BIRs* from 1270 to 2500 cm^{-1} (covering the silicate to water region) and from 3890 to 4000 cm^{-1} (upper end of the water region) (Figure 4). In the silicate region, the first *BIR* limit is fixed at the origin (0 cm^{-1}) whereas its second limit, and the extension and location of the intermediate *BIRs* (2nd and eventually 3rd) are variable. However, this method is equally strict and robust because it consists of placing small intermediate *BIRs* at spectral troughs and varying their extension to obtain the maximum silicate area that can be controlled in real time on the `SilicH2O` interface. The same criterion is applied to the second limit of the 1st *BIR*. We suggest to first place it at about 300–350 cm^{-1} and then move it backwards until the maximum area of the silicate peaks is reached. In our database, this limit varies in between 185 and 293 cm^{-1} and appears to roughly decrease with the degree of glass polymerization, that is inversely proportional to the non-bridging oxygens/tetrahedral ratio [NBO/T, estimated according to Giordano et al. 2020, Supplementary Material 1]. Indeed, the optimum position of this limit is 173–180 cm^{-1} for the haplogratites (NBO/T = 0.0), 185–200 cm^{-1} for the phonolite samples, (NBO/T = 0.24–0.35) and between 198 and 293 cm^{-1} for the most depolymerized glasses such as basalts, basaltic andesites, andesites, shoshonites, latites (NBO/T = 0.42–1.15) (Figure 4).

All plots in Figure 4 show the highest possible values of water and silicate areas (as also evident by comparison with the subtracted spectra of Figure 2), and the baselines at the *BIRs* limits looks a consistent extension of the baseline before and after the limits themselves. Despite having a fixed *BIR* at 2500 cm^{-1}, the baseline follows the pattern of the spectra to higher frequencies, intercepting the beginning of the water peak at 2700 cm^{-1} for the basalt, andesite, latite, and shoshonite (Figure 4B, 4C, 4E, 4F), ~2850 cm^{-1} for the haplogranite (Figure 4A) and ~3100 cm^{-1} for the phonolite (Figure 4D). The water peaks intercept the baseline at the end of the spectra at 3800–3850 cm^{-1} (Figure 4). In this region, an additional spectra correction (averaging by interpolation) is occasionally

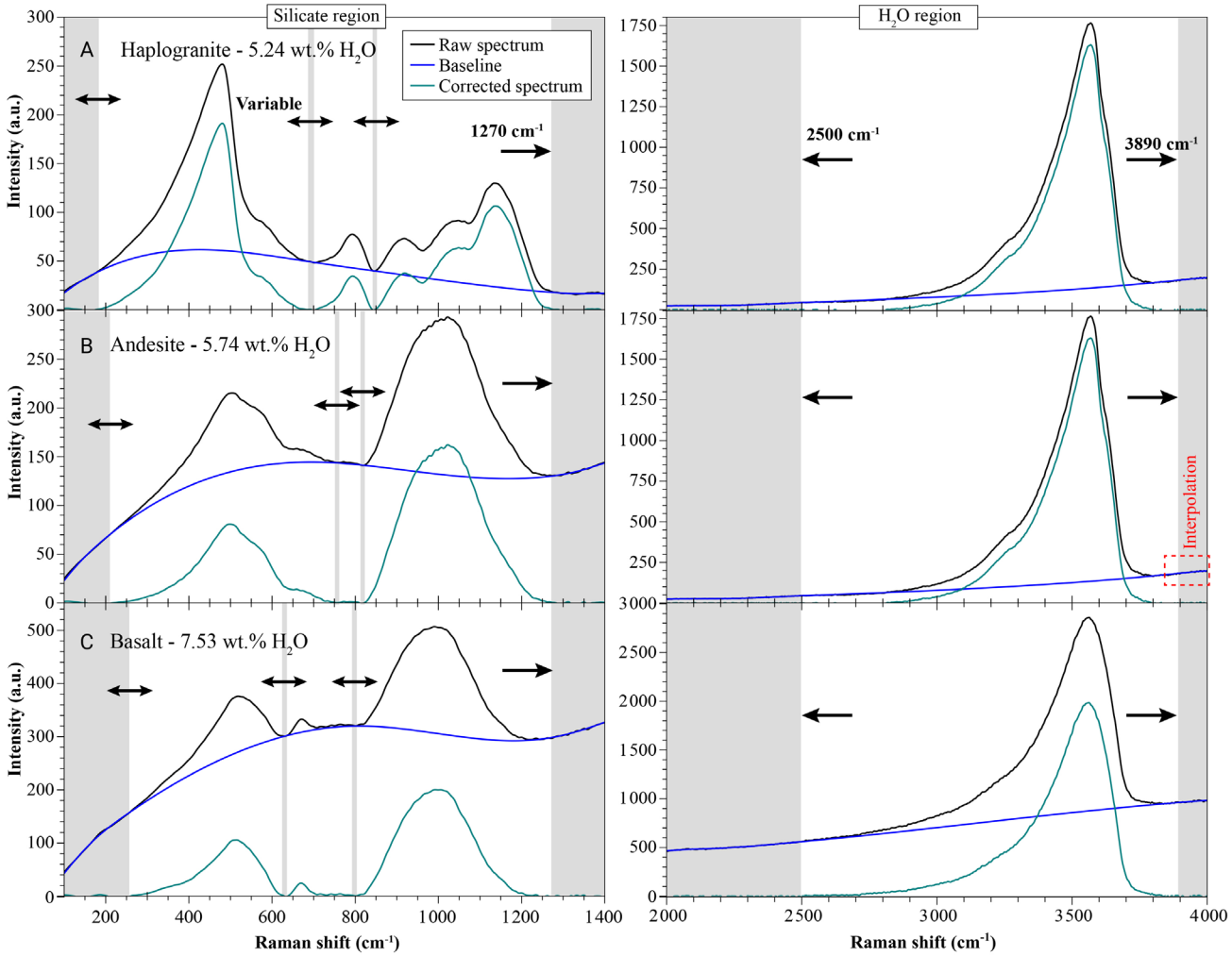

Figure 4: Application of the baseline subtraction method proposed in this work to the representative H_2O-bearing glass spectra of Figure 2A. Note that corrections by interpolation appear like dark blue baseline segments and were performed only in B, E, F. See Figure 2 for additional explanations. (Continued on next page.)

required (e.g. Figure 4B, 4E, and 4F). We noticed that a few of our spectra are noisy in this region. They show ups and downs that make the baseline bend respectively up and down underneath the water peak, resulting in underestimations and overestimations of the water area with respect to spectra of the same glass not showing this issue, leading to $R_{w/s}$ differences up to 0.5. Figure 5 reports two representative interpolation corrections of these zones and shows that the lower limit of the *BIR* (at 3890 cm^{-1}) falls in a small depression [A] and a shoulder [B], respectively. The application of this interpolation straightens the pattern of baseline below the H_2O peak, improving the consistency of these noisy spectra. The adoption of these interpolation depends on the ability and experience of the user. A favoured, alternative option is to discard these anomalously behaving spectra (to avoid any arbitrariness) and eventually acquire new ones.

4.2 H_2O-$R_{w/s}$ calibrations, uncertainty and error propagation

To decrease the density of data in some overpopulated H_2O-$R_{w/s}$ regions, that would determine a bias in the calibration equations [e.g. Ridolfi and Renzulli 2012] and reduce the uncertainty of water-$R_{w/s}$ calibration, we have split the glass database in two groups, a "high-quality" calibration dataset and a testing dataset (82 and 19 samples, respectively). The last includes glasses where the water content is just nominal (see Section 2.1) and others showing higher H_2O and/or $R_{w/s}$ uncertainties than analogous glasses (synthesized at the same P-T-fO_2 conditions and anhydrous composition, and having approximately the same H_2O content) in the calibration dataset (Supplementary Material 1).

Figure 6 reports the correlation of the H_2O and $R_{w/s}$ uncertainties (expressed as standard deviation in percentage, i.e. σ%) with the average amount of water [A] and $R_{w/s}$ [B], respectively. Similar to EPMA [Ridolfi et al. 2023], both water and $R_{w/s}$ show σ% values decreasing with the amount of measured (average) values by power relationships (black curve). The overall quality (precision) of our database is highlighted by the fact that most of the glasses fall below of the red power curve, representing the power relationships multiplied by a factor of two [e.g. Ridolfi et al. 2023]. This test indicates that the glasses are homogeneous and should be performed by any

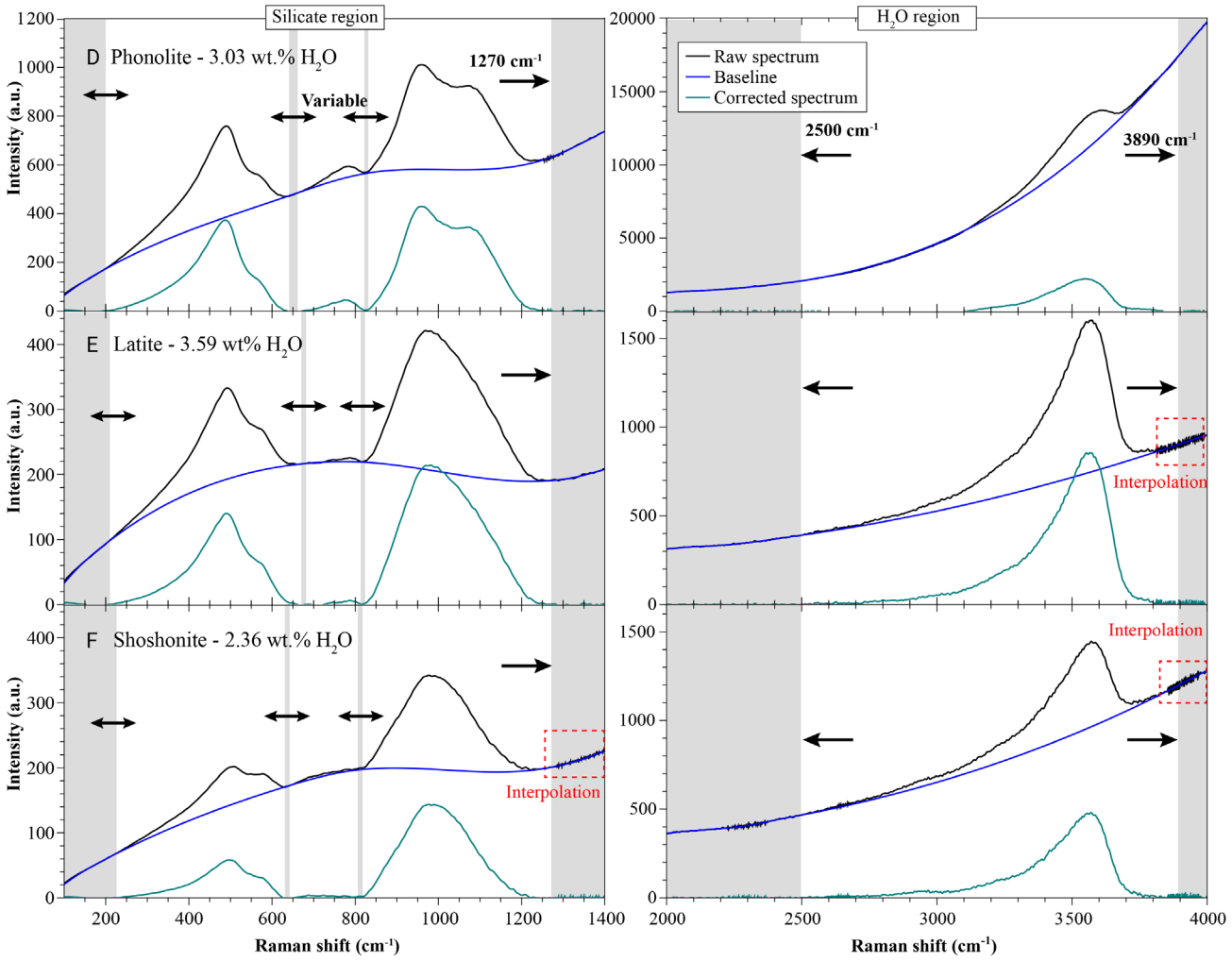

Figure 4: Continued.

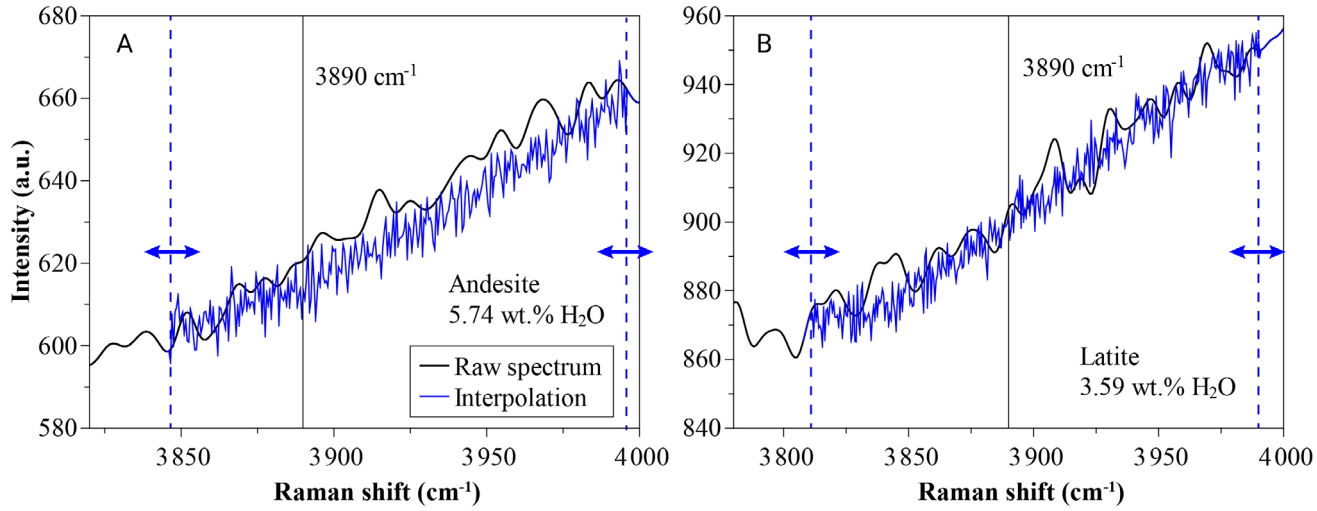

Figure 5: Intensity (a.u.) vs. Raman frequency shift (cm^{-1}) diagrams showing representative interpolation corrections at the end of the spectra, i.e. enlargements of Figure 4B [A] and 4E [B].The original and corrected spectra patterns are black and blue, respectively. The last is limited by the dashed blue lines and the blue double arrows indicate that this positions can be adjusted. The lower limit of the last fixed *BIR* is also shown (3890 cm^{-1}). See text for additional explanations.

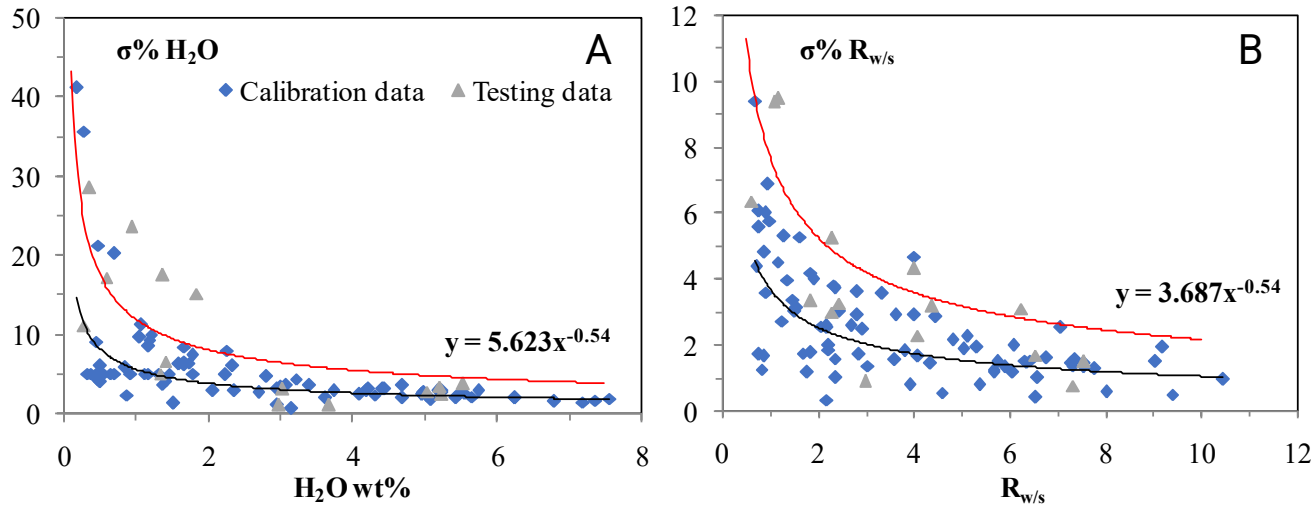

Figure 6: Plot of the relative uncertainties of [A] water and [B] $R_{w/s}$ determinations. [A] and [B] respectively report correlations of the standard deviation percentages of water (i.e. σ% H_2O = σ H_2O wt.% × 100/average H_2O wt.%) and $R_{w/s}$ (i.e. σ% $R_{w/s}$ = σ$R_{w/s}$ × 100/average $R_{w/s}$) with the average amounts of H_2O wt.% and $R_{w/s}$ of multiple determinations for each glass. In both diagrams, the correlations are reported by black curves and power equations. The red curves represent the power equations multiplied by a factor of two [e.g. Ridolfi et al. 2023].

user/lab to check the quality of their calibration glass standards and samples.

It is worth noting that the relative uncertainty of water determination is almost twice the $R_{w/s}$ uncertainty, as shown by the same exponential (-0.54) but different multiplication coefficient (5.62 and 3.69, respectively; Figure 6). In absolute terms, the average σ for the calibration data is 0.09 wt.% and 0.07 for H_2O and $R_{w/s}$, respectively, indicating high sensitivity and potential of Raman for measuring water in silicate glasses.

Figure 7 reports the correlations between the H_2O/(100–H_2O) and H_2O (wt.%) amounts, and the $R_{w/s}$ values. It is represented by the following equation:

$$\left(\frac{H_2O}{(100 - H_2O)}\right) = a_1 \cdot R_{w/s} + C_1; \quad (2)$$

where a_1 = 0.009 and C_1 = -0.004, R^2 = 0.984. It accounts for water content uncertainties in between -0.62 and +0.71 wt.%. The standard error of the estimate (σ_{est}) and the average error are 0.26 and 0.20 wt.%, respectively (Supplementary Material 1).

Empirically, H_2O (wt.%) and $R_{w/s}$ are better correlated by a polynomial relation (Figure 7B):

$$H_2O\ (wt.\%) = a_2 \cdot R^2_{w/s} + b_2 \cdot R_{w/s} + C_2; \quad (3)$$

where a_2= -0.009, b_2 = +0.882 and C_2 = -0.394; R^2 = 0.984. Equation 3 shows the same uncertainty range, σ_{est} and average error of Equation 2 (see above and Supplementary Material 1). The testing dataset results in errors from -0.5 to +0.6 wt.%, which are within the error ranges for both equations (see above), confirming the validity of the proposed methodology.

Both relations intercept the y-axis at negative values (c_1 = -0.004, accounting for an H_2O value of -0.37 wt.%; c_2 = -0.39 wt.% H_2O); as a consequence, their application at low H_2O values (<1 wt.% H_2O) involves high uncertainties (up to 100% relative) or may give negative values. This is most probably because the density of the calibration dataset is unbalanced, i.e. mostly made of glasses of the sub-alkaline series (i.e. basalt, basaltic andesite, andesite; Figure 7 and Supplementary Material 1). It is worth noting that forcing the equations to intercept the origin largely lowers the determination coefficients (R^2 = 0.974 and 0.977 for [A] and [B], respectively) and increases the uncertainty (σ_{est} 0.33 and 0.31 wt.% for [A] and [B], respectively), and hence it is not recommended. An additional issue is that both equations alway overestimate the water content of glasses with haplogranite (rhyolite) and shoshonite compositions by 0.2–0.7 wt.% (Figure 7; Supplementary Material 1) suggesting a compositional effect on the $R_{w/s}$ data. Indeed, shoshonites and haplogranites show lower [H_2O/(100–H_2O)]-$R_{w/s}$ and [H_2O wt.%]-$R_{w/s}$ relationships than those predicted by the overall correlations and equations (Figure 7).

According to the probability theory, general uncertainties (average σ) of 0.07 for $R_{w/s}$ and 0.09 wt.% for H_2O (see above) account for an error propagation of 0.16 wt.%. This value is lower than the calculated average error and σ_{est} of water determination for both equations (0.20 and 0.26 wt.%; see above and Supplementary Material 1), also suggesting a compositional/structural effect on the $R_{w/s}$ values.

In principle, these discrepancies could be due to an underestimation of the silicate area for the haplogranite and shoshonite glasses by the proposed spectra processing method, resulting in $R_{w/s}$ overestimations for these glasses. To test this hypothesis, we used an additional small BIR for the haplogranite spectrum at 960 cm^{-1} (see Figure 4A), we adopted only one *BIR* or no *BIRs* at the intermediate silicate region, and/or maintained fixed the higher limit of the 1st *BIR* at the beginning of the spectra (at 71–72 cm^{-1}) where the silicate area result maximum for the haplogranites. Nevertheless, any combination of

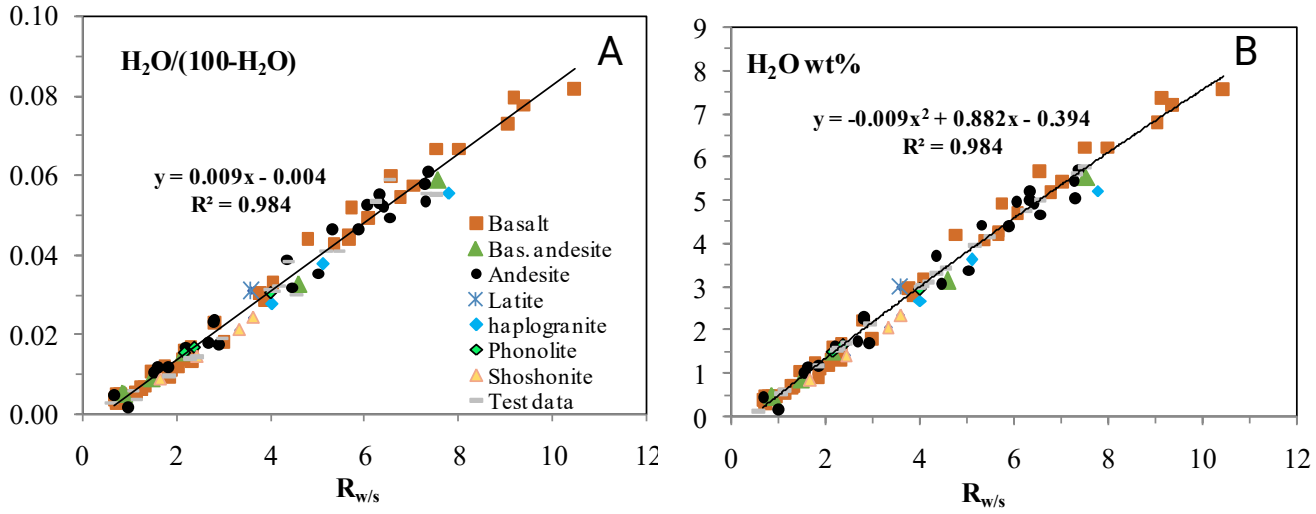

Figure 7: Water/silicate mass ratio [A] and H_2O wt.% [B] vs.$R_{w/s}$.

these constraints resulted in $H_2O/(100–H_2O)$ and H_2O wt.% - $R_{w/s}$ relations with lower R^2 (< 0.973), suggesting that the silicate area is correctly estimated with our baseline-subtraction method for the haplogranite and shoshonite glasses as well.

Another possibility is that the water peak area is overestimated for the haplogranite and shoshonite glasses. This can be corrected by moving their *BIR* limit at 2500 cm^{-1} to higher frequencies but this is user dependent and, thus, quite arbitrary . Attempts to move this fixed limit position for all glasses in our database to higher frequencies (up to 3100 cm^{-1}) always resulted in lower R^2 values of the $H_2O/(100–H_2O)$ and H_2O wt.% - $R_{w/s}$ correlations. All of this suggests that the proposed spectra processing method is robust, and to date it is the better constrained method to remove the background signal with the aid of applications such as `SilicH2O`.

5 Compositional effects and multivariate calibrations

Raman scattering is a response to molecule vibration when the material is excited by a laser, and not to its mass. Despite such a basic assumption, most authors nowadays investigate H_2O-bearing glasses by correlations of the ratio between the water and silicate areas ($R_{w/s}$) to the ratio between water and glass masses (i.e. $H_2O/(100–H_2O)$) and not molecular contents. For this reason, we analyzed the relationship between $R_{w/s}$ data and the hydrous and anhydrous glass parameters calculated on the 8 oxygen basis [e.g. Ridolfi et al. 2014, Supplementary Material 1].

5.1 Molecular ratios and formula parameters vs. $R_{w/s}$

Figure 8A reports the relationship between the H/Σcations (H atoms per 8-oxygens, hereafter p8O, divided by the sum of the remaining cations p8O) and $R_{w/s}$, in an analogous way to Figure 7A. The consequence is an increase in the differences between the different groups of glasses as shown by a decrease of R^2 from 0.983 (Figure 7A) to 0.979 (Figure 8A). These differences are better displayed in Figure 8B, showing the relationships between the H content (p8O) and $R_{w/s}$ and the correlation lines between the different groups of glasses. The most primitive glasses (basalts) show the highest slope of the H-$R_{w/s}$ correlation line (0.246), followed by the shoshonites (0.235), phonolites (0.232) and andesites (0.229). As expected, the haplogranites are the most anomalous ones and show a higher deviation with respect to the general trend, and the lowest slope of the correlation line (i.e. slope = 0.176).

This could suggest that the amount of silica (and Si p8O) is the main factor controlling the H-$R_{w/s}$ relationship. Nevertheless, silica concentration alone cannot explain this behavior, since phonolites and shoshonites show very similar slopes (0.232 and 0.235, respectively) despite having different SiO_2 contents (61.4 wt.% vs 52.7 wt.%). Furthermore, the degree of polymerization (NBO/T) fails to give a sound explanation to this behavior, since phonolites show an NBO/T of 0.1, closer to haplogranites (NBO/T = 0.0) than the rest of the glass samples (NBO/T ≥ 0.3; Figure 8C).

Among the tetrahedral forming cations calculated on the anhydrous basis (i.e. Si^{4+}, Ti^{4+}, Al^{3+}, Fe^{3+}), the sum of tetravalent ones shows a general decrease with the H-$R_{w/s}$ slope, but in this case phonolites show again a different behavior (Figure 8D). These phonolites stand out by their high amount of tetrahedral-forming trivalent cations (i.e. $R^{3+} = Al^{3+} + Fe^{3+}$, in particular aluminum; Supplementary Material 1). This is shown in Figure 8E, where the R^{3+} content (p8O) is plotted against $R_{w/s}$. The H-$R_{w/s}$ slope generally increases with R^{3+} and phonolites plot just above the shoshonites, although showing slightly lower slope (0.232 and 0.235 respectively). This small discrepancy is mostly due to the high amounts of pentavalent cations, i.e. P^{5+}, in the shoshonites (P_2O_5 = 1.3 wt.%), compared to those of the remaining samples ($P_2O_5 \leq 0.3$ wt.%) (Supplementary Material 1).

In fact, Figure 8F shows that the H-$R_{w/s}$ slope increases regularly with the sum of trivalent ($R^{3+} = Al^{3+} + Fe^{3+}$) and pentavalent ($R^{5+} = P^{5+}$) cations. To verify this hypothesis, we have divided the high-quality data in groups with different $R^{3+} + R^{5+}$ contents (independently of their classification), and

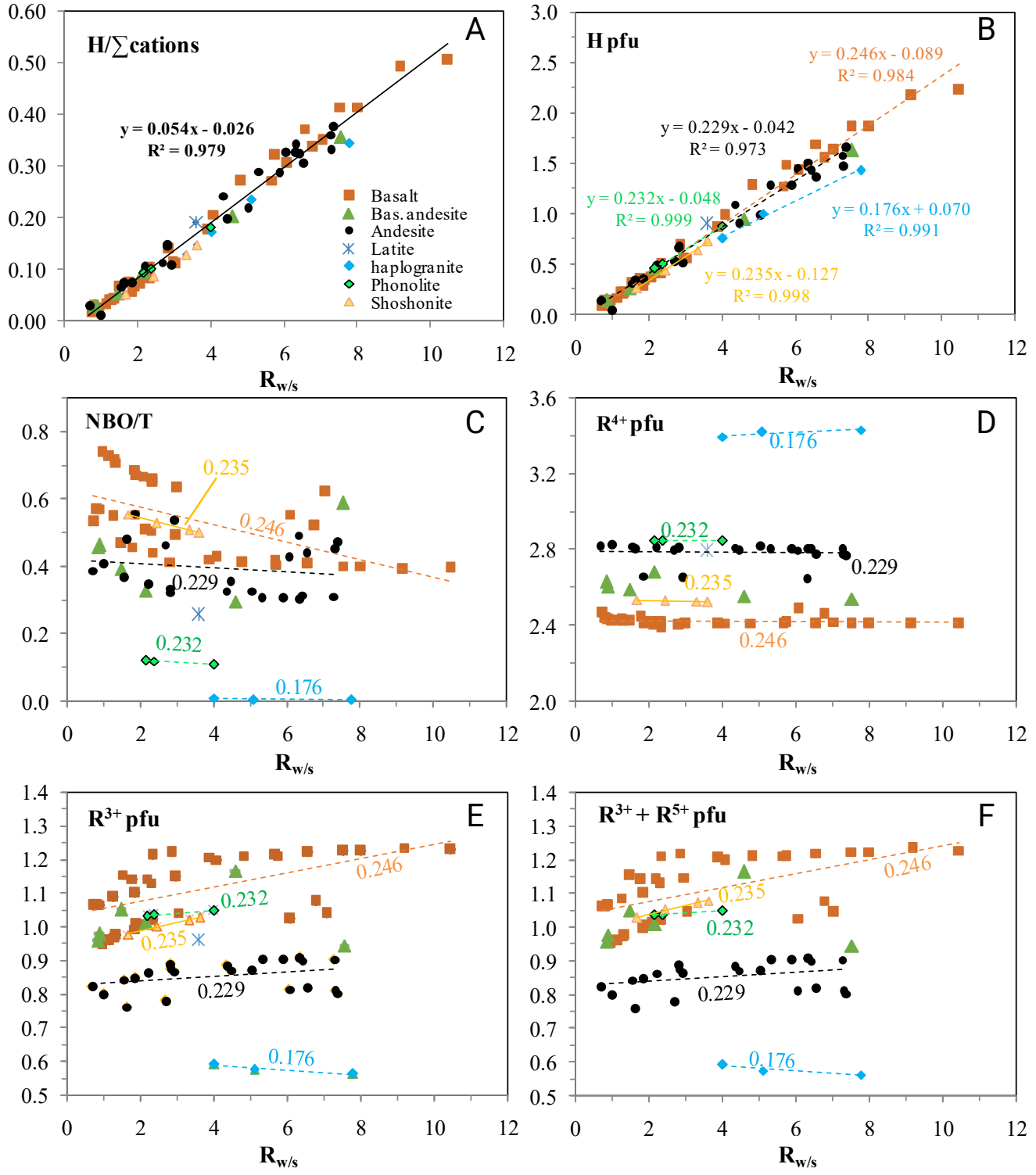

Figure 8: Representative correlations between compositional/structural parameters: [A] Hydrogen per 8-oxygens formula unit, hereafter H p8O, divided by the sum of the remaining cations, i.e. H/Σcations; [B] H p8O; [C] depolymerisation degree, i.e. NBO/T; [D] R^{4+} = Si^{4+} + Ti^{4+} p8O; [E] R^{3+}= Al^{3+} + Fe^{3+} p8O; [F] R^{3+} + R^{5+} = Al^{3+} + Fe^{3+} + P^{5+} p8O) and $R_{w/s}$ for the calibration (high-quality) glasses. In A, the correlation line among all calibration (high-quality) glasses is reported, together with its equation and determination coefficient. In B to F, the coloured-dashed lines show the correlations of some glass groups with labels having the same colour. In B, related equations and R^2 values are also shown with the same colour. C to F also reports the correlation slopes of B for the glass groups. See text for additional explanations.

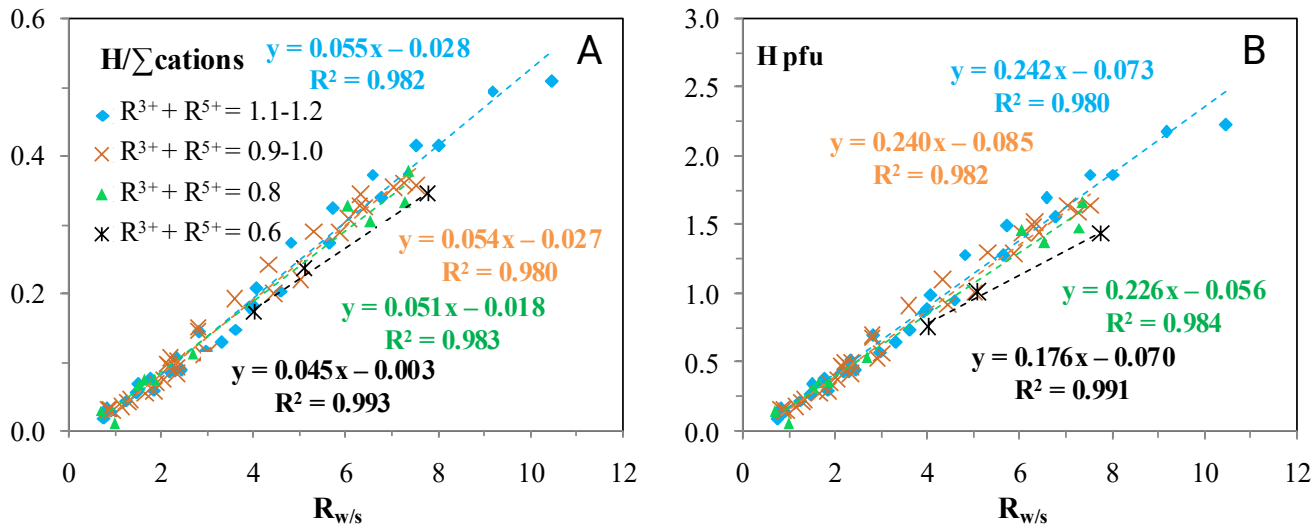

Figure 9: H/Σcations [A] and H p8O [B] vs. $R_{w/s}$ diagrams for the high-quality data grouped by their amount of R^{3+} + R^{5+} cations (p8O). See Figure 8 for additional explanations.

plotted them again in the H/Σcations and H (p8O) vs. $R_{w/s}$ diagrams (Figure 9).

It is observed that the slope of the H/Σcations-$R_{w/s}$ and H (p8O)-$R_{w/s}$ correlations increases invariably with the amount of R^{3+} + R^{5+}. Indeed, groups of glasses with amounts of R^{3+} + R^{5+} cations of 0.6, 0.8. 0.9–1.0 and 1.1–1.2 p8O have slopes of 0.045, 0.051, 0.054 and 0.055, respectively, and their correlation indicate rather high R^2 values (0.98–0.99). However, this insight needs confirmation and the extent of this variation (and the determination of an $R_{w/s}$ correcting coefficient for water determination) cannot be estimated easily. This is mostly because the amount of Fe^{3+} in the glasses of this work is not measured but estimated after a series of calculations based on two models that should be updated and/or refined [i.e. Burnham 1994; Jayasuriya et al. 2004]. The model of Jayasuriya et al. [2004], as well as all existing iron oxidation state applications, was calibrated with anhydrous glasses and its uncertainty with hydrous ones is unknown. The Burnham model, from which we calculated the water activity to estimate the effective fO_2 condition required for the application of any iron oxidation-state model (see Section 2.1), was calibrated for granitic melts and occasionally gives unrealistic a_{H2O} values (i.e. > 1) for high water contents and basic-intermediate glasses that were forced to 1 in this work. In order to test this overall procedure, we used the oxidation state of iron as determined by wet chemistry calorimetric measurements [Schuessler et al. 2008; Knipping et al. 2015] in the phonolites and shoshonites reported in this work [Fe^{2+}/Fe_{tot} = 0.3–0.4 and 0.7–0.9, respectively González-García et al. 2017; 2024]. This test indicates that the estimated Fe^{2+}/Fe_{tot} for the phonolites (0.5–0.7) and shoshonites (0.6–0.8) is systematically overestimated and underestimated, with Fe^{2+}/Fe_{tot} estimated minus measured values of +0.2 and -0.1, respectively. This systematicity is quite important because it suggests that the H_2O-$R_{w/s}$ relationship can be potentially adjusted through multivariate regression [e.g. Putirka et al. 1996; Putirka 2008; Ridolfi and Renzulli 2012; Ridolfi et al. 2014].

5.2 H_2O calibration accounting for $R_{w/s}$ and chemical composition

In this work we performed a large number of least-square multivariate regression analyses inputting $H_2O/(100-H_2O)$, H_2O wt.% and H p8O as dependent variable, and $R_{w/s}$, its squared value ($R^2_{w/s}$, to account for the polynomial relations; e.g. Figure 7B) as independent variables, together with the anhydrous (wt.% and p8O) composition of the glasses.

The best regression results directly involve H_2O wt.% (dependent variable), and independent variables such as $R_{w/s}$, $R^2_{w/s}$ and the anhydrous composition of the glasses (wt.%). They are characterized by the following equations:

$$\begin{aligned} H_2O\,\text{wt.\%} = {} & a_3 \cdot R^2_{w/s} + b_3 \cdot R_{w/s} + c_3 \cdot SiO_2 + d_3 \cdot TiO_2 \\ & + e_3 \cdot Al_2O_3 + f_3 \cdot Fe_2O_3 + g_3 \cdot FeO + h_3 \cdot MnO \\ & + i_3 \cdot MgO + j_3 \cdot CaO + k_3 \cdot Na_2O + l_3 \cdot K_2O \\ & + m_3 \cdot P_2O_5 + C_3; \end{aligned} \quad (4)$$

$$\begin{aligned} H_2O\,\text{wt.\%} = {} & a_4 \cdot R^2_{w/s} + b_4 \cdot R_{w/s} + c_4 \cdot SiO_2 + d_4 \cdot TiO_2 \\ & + e_4 \cdot Al_2O_3 + f_4 \cdot FeO_{tot} + g_4 \cdot MnO + h_4 \cdot MgO \\ & + i_4 \cdot CaO + j_4 \cdot Na_2O + k_4 \cdot K_2O + l_4 \cdot P_2O_5 + C_4. \end{aligned} \quad (5)$$

C_3 and C_4 are constants, and a_i to m_i are coefficients to be multiplied by the anhydrous glass compositions (SiO_2 wt.%, TiO_2 wt.% etc.; Supplementary Material 1), with estimated Fe_2O_3 and FeO content for Equation 4 and the measured total amount of iron oxide (i.e. FeO_{tot}) for Equation 5. R^2 and statistical uncertainties are slightly better for Equation 4 and they both intercept the origin when the estimated H_2O wt.% content is plotted against the measured one (Figure 10).

The diagrams of Figure 10 also show that these equations erase any compositional difference as both shoshonites and

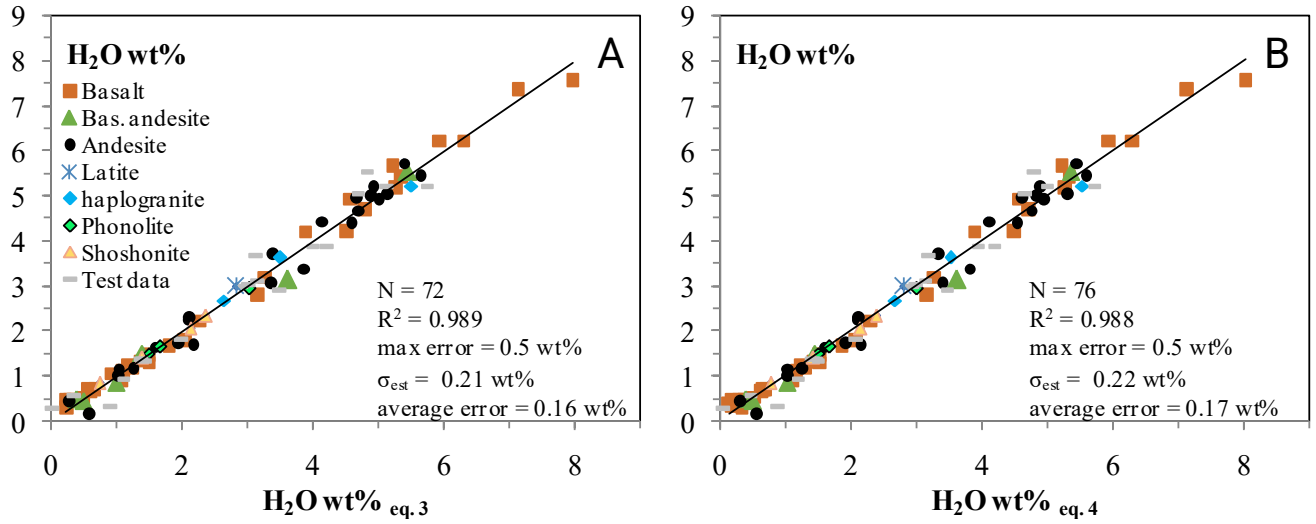

Figure 10: Correlation between the measured H_2O wt.% content and that estimated with equations 3 (A) and 4 (B). The black line reports this correlation among the high-quality (calibration) data. It corresponds to the 1:1 relationship. The test data are also plotted in both diagrams. The number of sample (N) and statistic values are reported for the calibration data only.

haplogranites straddle the correlation line. Overall the application of equations 4 and 5 brings the maximum uncertainty from ±0.7 to ±0.5 wt.%. Any bias due to the glass chemistry appears to be removed. For instance, the water content of all the haplogranite glasses is constantly overestimated with the compositionally-independent equations 2 and 3. The haplogranite with the higher water concentration (5.24 wt.%) shows an overestimation of 0.71 wt.%, 13.5% relative. In contrast, the application of equations 4 and 5 indicates an overestimation of 0.28–0.30 wt.% for this glass (only 5–6% relative) that is totally removed for the other haplogranites (Supplementary Material 1). Similarly, the application of equations 2 and 3 to some sub-group of basalts with similar composition (e.g. those having a label starting with M; Supplementary Material 1), constantly underestimates H_2O with errors up to 0.62 wt.% for water contents of 5.65 wt.% (11% relative; M30 sample). Such underestimation is reduced of about 30% with the application of equations 4 and 5. It is worth noting that the average error of equations 4 and 5 (0.16–0.17 wt.%) is comparable to that due to the error propagation theory (i.e. 0.16 wt.%; see Section 4.2). Although apparently tiny (0.03–0.04 wt.%), the improvement in σ_{est} of equations 4 and 5 is actually important because, in percentage terms, it accounts for an improvement of 12–15% (i.e. 0.03 and 0.04 wt.% × 100 / 0.26 wt.%) with respect to the compositionally-independent equations 2 and 3 (σ_{est} = 0.26 wt.%). The test glass data straddle the 1:1 correlation line in Figure 10 and, due to their lower quality, indicate higher uncertainties (σ_{est}= 0.33–0.34 wt.%, average error = 0.26 wt.%; see Supplementary Material 1 and Figure 10 for comparisons).

6 Conclusive remarks

The results reported in this work suggest that the Raman ratio between water and silicate regions (i.e. $R_{w/s}$) is affected by the glass composition (i.e. R^{3+} + R^{5+} amounts), and its effect cannot be compensated by only the use of a baseline subtraction procedure as previously suggested by other authors [e.g. Zajacz et al. 2005; Le Losq et al. 2012]. In contrast, the combination of Raman spectroscopy and EPMA data lead to an accurate calibration for *in-situ* measuring of water in glasses. Equation 4 is particularly useful for experimental glasses when the fO_2 and *P-T* conditions are accurately determined, while Equation 5 is recommended for *in-situ* water determination of natural glasses (e.g. matrix volcanic glasses and melt inclusions) as it only requires data from micro-Raman and routine EPMA analyses.

Given the empirical nature of both equations, they should be applied in the compositional (and H_2O wt.%) range of the calibration data. Outside this range the uncertainty of water determination is unpredictable [Ridolfi and Renzulli 2012; Ridolfi et al. 2014; Gorini et al. 2018; Ridolfi et al. 2018; Ridolfi 2021]. In addition to presenting the data of this work, Supplementary Material 1 can be used by other user/labs as a template to obtain their Raman calibration by entering their $R_{w/s}$, fO_2 and glass composition data.

The combination of EPMA and micro-Raman data for *in-situ* water determination has great potential for improvement. First, the sensitivity of Raman to water variation appears superior to that of KFT and FTIR determinations, as shown by its lower average uncertainty (e.g. Figure 6), so a meticulous use of only accurate KFT data may potentially reduce the error of both equations 4 and 5. Secondly, a confirmation of the influence of the oxidation state of iron on Raman measurements, and a consequent improvement of the calibration method, can be derived from a direct determination of the Fe^{2+}/Fe^{3+} ratio in glasses [Schuessler et al. 2008; Potapkin et al. 2012; Knipping et al. 2015; Zhang et al. 2018]. For this purpose, *in-situ* micro-techniques such as micro-Mössbauer spectroscopy [McCammon et al. 1991; Potapkin et al. 2012] and the promising EPMA "flank-method" [Hughes et al. 2018; Zhang et al. 2018] are preferable, given the small size of melt inclusions and glass matrix pools in experimental products and the need for reproducibility in petrological and volcanological studies.

Author Contributions

The analytical part of this paper was performed by both authors and other colleagues (see below) at LUH. FR conceived the research and performed most of the data processing tasks while DGG performed additional tests of the proposed methods.

Acknowledgements

This research was funded by the Deutsche Forschungsgemeinschaft (DFG) with a research grant to FR (code RI 3065/2-3). DGG acknowledges the Alexander von Humboldt Foundation for a Humboldt postdoctoral fellowship. L. Koch and F. Marxer (LUH) are kindly thanked for technical help, performing some measurements and profitable discussions.

Data Availability

All data presented in this work are reported in Supplementary Material 1, a .xlsx file operating in `Microsoft Excel` (`Office 2010`). Raw spectrum files are provided as Supplementary Material 2.

Copyright Notice

References

Aitchison, J. (1986). "The statistical analysis of compositional data". *Journal of the Royal Statistical Society: Series B (Methodological)* 44(2), pages 139–160. DOI: 10.1007/978-94-009-4109-0.

Almeev, R. R., F. Holtz, J. Koepke, and F. Parat (2012). "Experimental calibration of the effect of H_2O on plagioclase crystallization in basaltic melt at 200 MPa". *American Mineralogist* 97(7), pages 1234–1240. DOI: 10.2138/am.2012.4100.

Almeev, R. R., F. Holtz, J. Koepke, F. Parat, and R. E. Botcharnikov (2007). "The effect of H_2O on olivine crystallization in MORB: Experimental calibration at 200 MPa". *American Mineralogist* 92(4), pages 670–674. DOI: 10.2138/am.2007.2484.

Almeev, R. R., F. Holtz, A. A. Ariskin, and J.-I. Kimura (2013). "Storage conditions of Bezymianny Volcano parental magmas: results of phase equilibria experiments at 100 and 700 MPa". *Contributions to Mineralogy and Petrology* 166(5), pages 1389–1414. DOI: 10.1007/s00410-013-0934-x.

Bamber, E. C., D. Giordano, M. Masotta, F. Arzilli, F. Colle, D. González-García, V. de Assis Janasi, F. R. D. de Andrade, S. R. Vlach, M. R. Carroll, and D. B. Dingwell (2024). "Experimental constraints on the pre-eruptive conditions of the Caxias do Sul dacite: Implications for high temperature silicic volcanism of the Paraná Magmatic Province, Brazil". *Chemical Geology* 662(122236). DOI: 10.1016/j.chemgeo.2024.122236.

Behrens, H., V. Misiti, C. Freda, F. Vetere, R. E. Botcharnikov, and P. Scarlato (2009). "Solubility of H_2O and CO_2 in ultrapotassic melts at 1200 and 1250 °C and pressure from 50 to 500 MPa". *American Mineralogist* 94(1), pages 105–120. DOI: 10.2138/am.2009.2796.

Behrens, H., C. Romano, M. Nowak, F. Holtz, and D. B. Dingwell (1996). "Near-infrared spectroscopic determination of water species in glasses of the system $MAlSi_3O_8$ (M = Li, Na, K): an interlaboratory study". *Chemical Geology* 128(1-4), pages 41–63. DOI: 10.1016/0009-2541(95)00162-x.

Behrens, H., J. Roux, D. R. Neuville, and M. Siemann (2006). "Quantification of dissolved H_2O in silicate glasses using confocal microRaman spectroscopy". *Chemical Geology* 229(1-3), pages 96–112. DOI: 10.1016/j.chemgeo.2006.01.014.

Berndt, J., C. Liebske, F. Holtz, M. Freise, M. Nowak, D. Ziegenbein, W. Hurkuck, and J. Koepke (2002). "A combined rapid-quench and H_2-membrane setup for internally heated pressure vessels: Description and application for water solubility in basaltic melts". *American Mineralogist* 87 (11-12), pages 1717–1726. DOI: 10.2138/am-2002-11-1222.

Blundy, J. and K. Cashman (2008). "Petrologic reconstruction of magmatic system variables and processes". *Reviews in Mineralogy and Geochemistry* 69(1), pages 179–239. DOI: 10.2138/rmg.2008.69.6.

Blundy, J., K. Cashman, and M. Humphreys (2006). "Magma heating by decompression-driven crystallization beneath andesite volcanoes". *Nature* 443(7107), pages 76–80. DOI: 10.1038/nature05100.

Bonechi, B., M. Gaeta, C. Perinelli, P. Moschini, C. Romano, and A. Vona (2022). "Micro-Raman water calibration in ultrapotassic silicate glasses: Application to phono-tephrites and K-foidites of Colli Albani Volcanic District (Central Italy)". *Chemical Geology* 597(120816). DOI: 10.1016/j.chemgeo.2022.120816.

Botcharnikov, R., J. Koepke, F. Holtz, C. McCammon, and M. Wilke (2005). "The effect of water activity on the oxidation and structural state of Fe in a ferro-basaltic melt". *Geochimica et Cosmochimica Acta* 69(21), pages 5071–5085. DOI: 10.1016/j.gca.2005.04.023.

Botcharnikov, R., R. Almeev, J. Koepke, and F. Holtz (2008). "Phase relations and liquid lines of descent in hydrous ferrobasalt—implications for the Skaergaard intrusion and Columbia River flood basalts". *Journal of Petrology* 49(9), pages 1687–1727. DOI: 10.1093/petrology/egn043.

Burnham, C. W. (1994). "Development of the Burnham Model for prediction of H_2O *solubility in magmas*". *Reviews in mineralogy* 30, pages 123–123. DOI: 10.1515/9781501509674-009.

Cáceres, F., B. Scheu, K.-U. Hess, C. Cimarelli, J. Vasseur, M. Kaliwoda, and D. B. Dingwell (2021). "From melt to crystals: The effects of cooling on FeTi oxide nanolites crystallisation and melt polymerisation at oxidising conditions". *Chemical Geology* 563(120057). DOI: 10.1016/j.chemgeo.2021.120057.

Di Genova, D., D. Morgavi, K.-U. Hess, D. R. Neuville, N. Borovkov, D. Perugini, and D. B. Dingwell (2015). "Approximate chemical analysis of volcanic glasses using Ra-

man spectroscopy". *Journal of Raman Spectroscopy* 46(12), pages 1235–1244. DOI: 10.1002/jrs.4751.

Di Genova, D., S. Sicola, C. Romano, A. Vona, S. Fanara, and L. Spina (2017). "Effect of iron and nanolites on Raman spectra of volcanic glasses: A reassessment of existing strategies to estimate the water content". *Chemical Geology* 475, pages 76–86. DOI: 10.1016/j.chemgeo.2017.10.035.

Di Muro, A., N. Métrich, M. Mercier, D. Giordano, D. Massare, and G. Montagnac (2009). "Micro-Raman determination of iron redox state in dry natural glasses: Application to peralkaline rhyolites and basalts". *Chemical Geology* 259(1–2), pages 78–88. DOI: 10.1016/j.chemgeo.2008.08.013.

Gaetani, G. A., J. A. O'Leary, N. Shimizu, C. E. Bucholz, and M. Newville (2012). "Rapid reequilibration of H_2O and oxygen fugacity in olivine-hosted melt inclusions". *Geology* 40(10), pages 915–918. DOI: 10.1130/g32992.1.

Giordano, D., D. González-García, J. K. Russell, S. Raneri, D. Bersani, L. Fornasini, D. Di Genova, S. Ferrando, M. Kaliwoda, P. P. Lottici, M. Smit, and D. B. Dingwell (2020). "A calibrated database of Raman spectra for natural silicate glasses: implications for modelling melt physical properties". *Journal of Raman Spectroscopy* 51(9), pages 1822–1838. DOI: 10.1002/jrs.5675.

González-García, D., H. Behrens, M. Petrelli, F. Vetere, D. Morgavi, C. Zhang, and D. Perugini (2017). "Water-enhanced interdiffusion of major elements between natural shoshonite and high-K rhyolite melts". *Chemical Geology* 466, pages 86–101. DOI: 10.1016/j.chemgeo.2017.05.023.

González-García, D., D. Giordano, A. Allabar, F. Andrade, L. Polo, V. Janasi, A. Lucchetti, K.-U. Hess, C. De Campos, and D. Dingwell (2021). "Retrieving dissolved H_2O content from micro-Raman spectroscopy on nanolitized silicic glasses: Application to volcanic products of the Paraná Magmatic Province, Brazil". *Chemical Geology* 567(120058). DOI: 10.1016/j.chemgeo.2021.120058.

González-García, D., D. Giordano, J. K. Russell, and D. B. Dingwell (2020). "A Raman spectroscopic tool to estimate chemical composition of natural volcanic glasses". *Chemical Geology* 556(119819). DOI: 10.1016/j.chemgeo.2020.119819.

González-García, D., M. Petrelli, H. Behrens, F. Vetere, L. A. Fischer, D. Morgavi, and D. Perugini (2018). "Diffusive exchange of trace elements between alkaline melts: Implications for element fractionation and timescale estimations during magma mixing". *Geochimica et Cosmochimica Acta* 233, pages 95–114. DOI: 10.1016/j.gca.2018.05.003.

González-García, D., F. Pohl, F. Marxer, S. Krasheninnikov, R. Almeev, and F. Holtz (2024). "Chemical interdiffusion between Na-series tephritic and phonolitic melts with different H_2O content, temperature, and oxygen fugacity values". *European Journal of Mineralogy* 36(4), pages 623–640. DOI: 10.5194/ejm-36-623-2024.

Gorini, A., F. Ridolfi, F. Piscaglia, M. Taussi, and A. Renzulli (2018). "Application and reliability of calcic amphibole thermobarometry as inferred from calc-alkaline products of active geothermal areas in the Andes". *Journal of Volcanology and Geothermal Research* 358, pages 58–76. DOI: 10.1016/j.jvolgeores.2018.03.018.

Hirschmann, M. M., M. S. Ghiorso, F. A. Davis, S. M. Gordon, S. Mukherjee, T. L. Grove, M. Krawczynski, E. Medard, and C. B. Till (2008). "Library of Experimental Phase Relations (LEPR): A database and Web portal for experimental magmatic phase equilibria data". *Geochemistry, Geophysics, Geosystems* 9(Q03011). DOI: 10.1029/2007gc001894.

Hughes, E. C., B. Buse, S. L. Kearns, J. D. Blundy, G. Kilgour, H. M. Mader, R. A. Brooker, R. Balzer, R. E. Botcharnikov, D. Di Genova, R. R. Almeev, and J. M. Riker (2018). "High spatial resolution analysis of the iron oxidation state in silicate glasses using the electron probe". *American Mineralogist* 103(9), pages 1473–1486. DOI: 10.2138/am-2018-6546CCBY.

Humphreys, M. C., S. L. Kearns, and J. D. Blundy (2006). "SIMS investigation of electron-beam damage to hydrous, rhyolitic glasses: Implications for melt inclusion analysis". *American Mineralogist* 91(4), pages 667–679. DOI: 10.2138/am.2006.1936.

Jayasuriya, K. D., H. S. O'Neill, A. J. Berry, and S. J. Campbell (2004). "A Mössbauer study of the oxidation state of Fe in silicate melts". *American Mineralogist* 89(11–12), pages 1597–1609. DOI: 10.2138/am-2004-11-1203.

Knipping, J. L., H. Behrens, M. Wilke, J. Göttlicher, and P. Stabile (2015). "Effect of oxygen fugacity on the coordination and oxidation state of iron in alkali bearing silicate melts". *Chemical Geology* 411, pages 143–154. DOI: 10.1016/j.chemgeo.2015.07.004.

Koch, L., R. R. Almeev, S. A. Linsler, F. Marxer, and F. Holtz (2025). "The effect of H_2O on the crystallization of orthopyroxene in a high-Mg andesitic melt". *American Mineralogist, in press*. DOI: 10.2138/am-2024-9593.

Konzett, J., T. Schneider, L. Nedyalkova, C. Hauzenberger, F. Melcher, A. Gerdes, and M. Whitehouse (2018). "Anatectic granitic pegmatites from the Eastern Alps: A case of variable rare-metal enrichment during high-grade regional metamorphism – I: Mineral assemblages, geochemical characteristics, and emplacement ages". *The Canadian Mineralogist* 56(4), pages 555–602. DOI: 10.3749/canmin.1800008.

Le Losq, C., D. R. Neuville, R. Moretti, and J. Roux (2012). "Determination of water content in silicate glasses using Raman spectrometry: Implications for the study of explosive volcanism". *American Mineralogist* 97(5–6), pages 779–790. DOI: 10.2138/am.2012.3831.

Leschik, M., G. Heide, G. H. Frischat, H. Behrens, M. Wiedenbeck, N. Wagner, K. Heide, H. Geißler, and U. Reinholz (2004). "Determination of H_2O and D_2O contents in rhyolitic glasses". *Physics and Chemistry of Glasses* 45 (4), pages 238–251.

Long, D. A. (1977). *Raman Spectroscopy*. New York: McGraw-Hill.

McCammon, C. A., V. Chaskar, and G. G. Richards (1991). "A technique for spatially resolved Mossbauer spectroscopy applied to quenched metallurgical slags". *Measurement Science and Technology* 2(7), pages 657–662. DOI: 10.1088/0957-0233/2/7/014.

Mercier, M., A. Di Muro, D. Giordano, N. Métrich, P. Lesne, M. Pichavant, B. Scaillet, R. Clocchiatti, and G. Montagnac

(2009). "Influence of glass polymerisation and oxidation on micro-Raman water analysis in alumino-silicate glasses". *Geochimica et Cosmochimica Acta* 73(1), pages 197–217. DOI: 10.1016/j.gca.2008.09.030.

Metrich, N. and P. J. Wallace (2008). "Volatile Abundances in Basaltic Magmas and Their Degassing Paths Tracked by Melt Inclusions". *Reviews in Mineralogy and Geochemistry* 69(1), pages 363–402. DOI: 10.2138/rmg.2008.69.10.

Mollo, S., J. Blundy, P. Scarlato, S. P. De Cristofaro, V. Tecchiato, F. Di Stefano, F. Vetere, F. Holtz, and O. Bachmann (2018). "An integrated P-T-H_2O-lattice strain model to quantify the role of clinopyroxene fractionation on REE+Y and HFSE patterns of mafic alkaline magmas: Application to eruptions at Mt. Etna". *Earth-Science Reviews* 185, pages 32–56. DOI: 10.1016/j.earscirev.2018.05.014.

Moore, G. (2008). "Interpreting H_2O and CO_2 contents in melt inclusions: Constraints from solubility experiments and modeling". *Reviews in Mineralogy and Geochemistry* 69(1), pages 333–362. DOI: 10.2138/rmg.2008.69.9.

Morgan VI, G. B. and D. London (2005). "Effect of current density on the electron microprobe analysis of alkali aluminosilicate glasses". *American Mineralogist* 90(7), pages 1131–1138. DOI: 10.2138/am.2005.1769.

Potapkin, V., A. I. Chumakov, G. V. Smirnov, J.-P. Celse, R. Rüffer, C. McCammon, and L. Dubrovinsky (2012). "The ^{57}Fe synchrotron Mössbauer source at the ESRF". *Journal of Synchrotron Radiation* 19(4), pages 559–569. DOI: 10.1107/s0909049512015579.

Putirka, K., M. Johnson, R. Kinzler, J. Longhi, and D. Walker (1996). "Thermobarometry of mafic igneous rocks based on clinopyroxene-liquid equilibria, 0-30 kbar". *Contributions to Mineralogy and Petrology* 123(1), pages 92–108. DOI: 10.1007/s004100050145.

Putirka, K. D. (2008). "Thermometers and barometers for volcanic systems". *Reviews in Mineralogy and Geochemistry* 69(1), pages 61–120. DOI: 10.2138/rmg.2008.69.3.

Ridolfi, F. (2021). "Amp-TB2: An updated model for valcic amphibole thermobarometry". *Minerals* 11(3), page 324. DOI: 10.3390/min11030324.

Ridolfi, F., R. R. Almeev, A. Y. Ozerov, and F. Holtz (2023). "Amp-TB2 protocol and its application to amphiboles from recent, historical and pre-historical eruptions of the Bezymianny Volcano, Kamchatka". *Minerals* 13(1394). DOI: 10.3390/min13111394.

Ridolfi, F., R. Braga, B. Cesare, A. Renzulli, D. Perugini, and S. Del Moro (2016). "Unravelling the complex interaction between mantle and crustal magmas encoded in the lavas of San Vincenzo (Tuscany, Italy). Part I: Petrography and Thermobarometry". *Lithos* 244, pages 218–232. DOI: 10.1016/j.lithos.2015.09.029.

Ridolfi, F. and A. Renzulli (2012). "Calcic amphiboles in calc-alkaline and alkaline magmas: thermobarometric and chemometric empirical equations valid up to 1,130° C and 2.2 GPa". *Contributions to Mineralogy and Petrology* 163, pages 877–895. DOI: 10.1007/s00410-011-0704-6.

Ridolfi, F., A. Renzulli, and A. Acosta-Vigil (2014). "On the stability of magmatic cordierite and new thermobarometric equations for cordierite-saturated liquids". *Contributions to Mineralogy and Petrology* 167(4). DOI: 10.1007/s00410-014-0996-4.

Ridolfi, F., A. Renzulli, and M. Puerini (2010). "Stability and chemical equilibrium of amphibole in calc-alkaline magmas: an overview, new thermobarometric formulations and application to subduction-related volcanoes". *Contributions to Mineralogy and Petrology* 160(1), pages 45–66. DOI: 10.1007/s00410-009-0465-7.

Ridolfi, F., A. Zanetti, A. Renzulli, D. Perugini, F. Holtz, and R. Oberti (2018). "AMFORM, a new mass-based model for the calculation of the unit formula of amphiboles from electron microprobe analyses". *American Mineralogist* 103(7), pages 1112–1125. DOI: 10.2138/am-2018-6385.

Schiavi, F., N. Bolfan-Casanova, A. C. Withers, E. Médard, M. Laumonier, D. Laporte, T. Flaherty, and A. Gómez-Ulla (2018). "Water quantification in silicate glasses by Raman spectroscopy: Correcting for the effects of confocality, density and ferric iron". *Chemical Geology* 483, pages 312–331. DOI: 10.1016/j.chemgeo.2018.02.036.

Schuessler, J. A., R. E. Botcharnikov, H. Behrens, V. Misiti, and C. Freda (2008). "Amorphous materials: Properties, structure, and durability: Oxidation state of iron in hydrous phono-tephritic melts". *American Mineralogist* 93(10), pages 1493–1504. DOI: 10.2138/am.2008.2795.

Shea, T., E. Hellebrand, L. Gurioli, and H. Tuffen (2014). "Conduit- to localized-scale degassing during Plinian eruptions: Insights from major element and volatile (Cl and H_2O) analyses within Vesuvius AD 79 pumice". *Journal of Petrology* 55(2), pages 315–344. DOI: 10.1093/petrology/egt069.

Shishkina, T., R. Botcharnikov, F. Holtz, R. Almeev, and M. Portnyagin (2010). "Solubility of H_2O- and CO_2-bearing fluids in tholeiitic basalts at pressures up to 500 MPa". *Chemical Geology* 277(1–2), pages 115–125. DOI: 10.1016/j.chemgeo.2010.07.014.

Thomas, S.-M., R. Thomas, P. Davidson, P. Reichart, M. Koch-Müller, and G. Dollinger (2008). "Application of Raman spectroscopy to quantify trace water concentrations in glasses and garnets". *American Mineralogist* 93(10), pages 1550–1557. DOI: 10.2138/am.2008.2834.

Tu, C., Z.-Y. Meng, X.-Y. Gao, and L. Zhang (2023). "Quantification of water content and speciation in synthetic rhyolitic glasses: Optimising the analytical method of confocal Raman spectrometry". *Geostandards and Geoanalytical Research* 47(3), pages 549–567. DOI: 10.1111/ggr.12490.

Van Gerve, T. D. and O. Namur (2023). "SilicH_2O: a graphical user interface for processing silicate glass Raman spectra and quantifying H_2O". *Volcanica* 6(2), pages 405–413. DOI: 10.30909/vol.06.02.405413.

Webster, J. D., B. De Vivo, and C. Tappen (2003). "Volatiles, magmatic degassing and eruptions of Mt. Somma-Vesuvius: Constraints from silicate melt inclusions, Cl and H_2O solubility experiments and modeling". *Melt Inclusions in Volcanic Systems - Methods, Applications and Problems*. Elsevier, pages 207–226. DOI: 10.1016/s1871-644x(03)80031-1.

Zajacz, Z., W. Halter, W. J. Malfait, O. Bachmann, R. J. Bodnar, M. M. Hirschmann, C. W. Mandeville, Y. Morizet, O. Mün-

tener, P. Ulmer, et al. (2005). "A composition-independent quantitative determination of the water content in silicate glasses and silicate melt inclusions by confocal Raman spectroscopy". *Contributions to Mineralogy and Petrology* 150, pages 631–642. DOI: 10.1007/s00410-005-0040-9.

Zhang, C., R. R. Almeev, E. C. Hughes, A. A. Borisov, E. P. Wolff, H. E. Höfer, R. E. Botcharnikov, and J. Koepke (2018). "Electron microprobe technique for the determination of iron oxidation state in silicate glasses". *American Mineralogist* 103(9), pages 1445–1454. DOI: 10.2138/am-2018-6437.

Zhang, Z.-M., S. Chen, Y.-Z. Liang, Z.-X. Liu, Q.-M. Zhang, L.-X. Ding, F. Ye, and H. Zhou (2010). "An intelligent background-correction algorithm for highly fluorescent samples in Raman spectroscopy". *Journal of Raman spectroscopy* 41(6), pages 659–669. DOI: 10.1002/jrs.2500.